Interaction Forces Between Phase Separated Lipid Membranes

By

SHAOLONG LIU

B.S. (Zhejiang University, P. R. China) 2012

THESIS

Submitted in partial satisfaction of the requirements for the degree of

MASTER OF SCIENCE

in

Chemical Engineering

in the

OFFICE OF GRADUATE STUDIES

of the

UNIVERSITY OF CALIFORNIA

DAVIS

Approved:

_____

Tonya Kuhl, Chair

_____

Marjorie Longo

_____

Ting Guo

Committee in Charge

2014

Contents

Abstract

Mixtures of saturated and doubly unsaturated lipids phase separate into solid phase domains in a continuous fluid phase. The surface force apparatus (SFA) was utilized to measure the interaction force profile between these nearly ideally phase separated membranes. Two membrane compositions were studied: 1:1 and 3:7 dipalmitoyl-sn-glycero-3-phosphoethanolamine:dioleoyl-sn-glycero-3-phosphocholine (DPPE:DOPC). The measured force profile could be correlated to the contributions of solid-solid, solid-fluid, and fluid-fluid membrane domains interacting in the contract region between the opposing membranes. In particular, the adhesion between the membranes was well described by mapping the van der Waals attraction of the different domain contributions. No additional attraction due to hydrophobic mismatch due to domain boundaries was detected. In addition, a weak, long-range electrostatic repulsion was detected due to the presence of charged, contaminant lipid species in the membrane (~1/100 lipids). The membrane domain morphology was characterized by fluorescence microscopy (FM) and atomic force microscopy (AFM) and correlated to the measured membrane interaction profile for two membrane compositions.

Acknowledgment

Foremost, I would like to express my sincere gratitude to my advisor Prof. Tonya L. Kuhl for the continuous support of my Master's study and research, for her patience, motivation, enthusiasm, and immense knowledge. Her guidance helped me in all the time of research and writing of this thesis. I could not have imagined having a better advisor and mentor for my graduate study.

Besides my advisor, I would like to thank the rest of my thesis committee: Prof. Marjorie Longo, and Prof. Ting Guo, for their encouragement, and insightful comments.

I thank my fellow labmates in our research group: James Kurniawan for the guidance of every single detail in the beginning of my research and help with both experiments and analysis of data, Daniel Kienle for assistance with SFA experimental setups, Joao Ventrici for implementing AFM experiments with patience, Christy Turcios, Miguel Turcios, Araceli Almeida and Hilary Chan for assisting with sample preparation, isotherm experiments and fluorescence measurements, for the stimulating discussions, and for all the fun we have had in the last two years.

Last but not the least, I would like to thank my family: my parents Run Zhang and Jushi Liu, for giving birth to me at the first place and supporting me spiritually throughout my life.

Introduction

1.1 Supported lipid bilayer membranes

Cell membranes, consisting largely of a lipid bilayer, are vital components of all living systems. Many important biological processes, including cell-cell communication, metabolisms, nutrients absorption, etc., are regulated at membrane surfaces. The complexity of biological membranes and their interactions with intra- and extracellular networks make direct investigations difficult.[1] For this reason, so called solid-supported membranes have been widely used to unravel the physical and chemical characteristics of membranes and how these contribute to membrane functions. Model lipid membrane systems of just a few molecular constituents have been studied for decades in an attempt to elucidate the fundamental thermodynamic and physical properties of cellular membranes. Although far from representing the complexity of real biological systems, such simplified systems allow focused studies on specific interactions and still display different ordered states, including solid, liquid disordered (Ld), liquid ordered (Lo) phases, and the coexistence of phases. These solid substrates supported phospholipid bilayers have been the most commonly used cell-surface model to gain insight into membrane-membrane interactions.[2-7]

By directly depositing lipid layers using methods like Langmuir-Blodgett (LB) deposition, the model lipid membranes maintain excellent mechanical stability without losing their fluid nature.[2, 8] The maintaining fluidity and excellent stability enable the use of many analytical methods that are impossible or difficult to use with a freely floating system. Many methods request the use of mechanical probing

techniques which require a direct physical interaction with the sample. For example, atomic force microscopy (AFM) has been used to image lipid phase separation[9], membrane morphology and protein assembly.[10] Another example using probe to study binding kinetics at the bilayer surface is quartz crystal microbalance (QCM).[11] The solid substrates supported lipid bilayer membranes enable such techniques to be used in studying the properties of membranes, which is hardly achievable in a cell or vesicle is relatively soft and would drift and fluctuate over time. Many modern fluorescence microscopy techniques also require a rigidly-supported planar surface. For example, extremely sensitive measurement of analyte binding and bilayer optical properties can be offered by evanescent field methods such as total internal reflection fluorescence microscopy (TIRF) and surface plasmon resonance (SPR) or optical interference such as fluorescence interference contrast microscopy (FLIC) and reflection interference contrast microscopy (RICM).[12]

One of the most primary drawbacks of supported lipid membranes is the possibility of unwanted interactions with the substrate. Although supported bilayers generally do not directly touch the substrate surface, they are separated by only a very thin water gap. The membrane–substrate distance is usually not sufficiently large to avoid direct contact between transmembrane proteins incorporated in the membrane and the solid surface. It will not be a dramatic problem for protein-free membrane system since only the protein will be denatured on the thin gap by touching the substrate surface and therefore lose all functionalities.[13] This problem also can be solved by adding soft polymeric materials between the membrane and solid substrates.[14-16]

1.2 Interactions between cell membranes

Interactions between cell membranes have been studied for decades of years due to its importance to reveal developmental processes involving changes in polarity, differentiation, division, death and migration. Biophysical studies on membrane interactions have been focused on illuminating the fundamental thermodynamic and physical properties of cell membrane by using model membrane systems with reduced complexity. Importantly, such simplified systems maintain most of properties of intact cell interactions and still display different ordered states, including gel, fluid and coexistence of gel and fluid phases. One of the most important interactions between cell membranes is membrane adhesion. Having a good understanding of membrane adhesion will help reveal the secret of cell communication, as well as design of drug for disease therapy. It is believed that membrane adhesion is governed by the interplay of specific interactions, generic interactions and membrane elasticity. Lock and key models between ligand and receptor molecules embedded in the cell membranes are the most famous examples of specific interactions. The ligand-receptor pairs promote the adhesion of membranes by pulling together opposing membranes in closer contact with a binding energy of ~ $35k_BT$.

For two neutral membranes with distance l, the total generic interaction potential energy per unit area[17-24] is given by

$$F_{tot}(l) = F_{hyd}(l) + F_{vdW}(l) + F_{und}(l) \qquad \text{(Eq.1)}$$

which consists of hydration energy, van der Walls interaction energy and undulation interaction energy.

The hydration energy, $F_{hyd}(l)$, has the empirical form[24]

$$F_{hyd}(l) = A_h \exp\left(\frac{-l}{\lambda_h}\right) \qquad \text{(Eq.2)}$$

with typical values of $A_h \cong 0.2$ J/m^2 and $\lambda_h \cong 0.3$ nm. The van der Walls interaction energy[24] is given by

$$F_{vdW}(l) = -\frac{W}{12\pi}\left[\frac{1}{l^2} - \frac{2}{(l+\delta)^2} + \frac{1}{(l+2\delta)^2}\right] \qquad \text{(Eq.3)}$$

where $W \cong 10^{-22}$ J, $\delta \cong 5$ nm.[23] The undulation interaction energy in the presence of membrane tension, τ, is expressed by

$$F_{und}(l) = c_{und}\frac{\tau k_B T}{\kappa}\left(\frac{l_\tau}{l}\right)^{\frac{1}{4}} \qquad \text{(Eq.4)}$$

where c_{und} is the dimensionless prefactor that determines the strength of the fluctuation-induced-interaction.[24]

Phase separation has been found to greatly enhance membrane adhesion in freely suspended system due to meta-fused states.[25] Hemifusion models were developed to explain the enhanced adhesion as a result of mixing of lipids with negative and zero spontaneous curvatures. Although these models can explain the phenomena for giant vesicles, interaction between supported phase separated membranes, especially some fundamental properties of micro-domains in membrane remaining obscure, including

their size and stability[26, 27] and physical properties.[28, 29]

1.3 Methods in investigating membrane-membrane interactions

Development on techniques highly helped to better investigate membrane interactions. Atomic force microscopy (AFM), one of the most widely used techniques in terms of supported membranes, allows for measurements of domain height due to alterations in the packing and composition of the domains.[30] However AFM is barely used to measure membrane-membrane interactions because of difficulties in forming membrane on silicon nitride tips.[31, 32] Fluorescence microscopy (FM) enables to profile membrane domains as a function of surface pressure, composition and temperature[33, 34] to investigate domain sizes and stabilities. Similarly as AFM, FM lacks possibilities in measuring membrane-membrane interactions. The most widely used and versatile technique for measuring membrane-membrane interactions is the surface force apparatus (SFA), providing a visualization of the area of supported membrane contact and profiling forces as a function of membrane separation with 1 Å resolution in distance and 10 pN resolution in force.[35-38]

The SFA technique has been used extensively to measure interaction forces between surfaces.[39-41] Before SFA was developed, long-range attractive forces between highly polished glass and quartz plates can be measured. With the restriction of cleanness (i.e. presence of dust particles) and surface roughness (limitation on polishing techniques), small distance (< 20 nm) became difficult.[42] After SFA was first created in 1969 by Tabor and Winterton, separation within 5 – 30 nm with a 3Å distance resolution can be measurable.[43] Recent version of SFA has been highly

improved in resolution of both separation and force measurements, making sub-nanometer distance measurement possible to discover membrane-membrane interactions. Figure 1.1 is the schematic picture of SFA Mark Ⅱ, which is commonly used to measure forces between two molecularly smooth surfaces.

With the help of these techniques, details on membrane-membrane interaction can be discovered deeply and thoroughly to benefit the design of drug delivery and knowledge on cell communication. In spite of huge amount of work has been done on this area, little attention has been paid on domain morphology and its influence on membrane interaction in substrate-supported phase separated lipid membrane system.

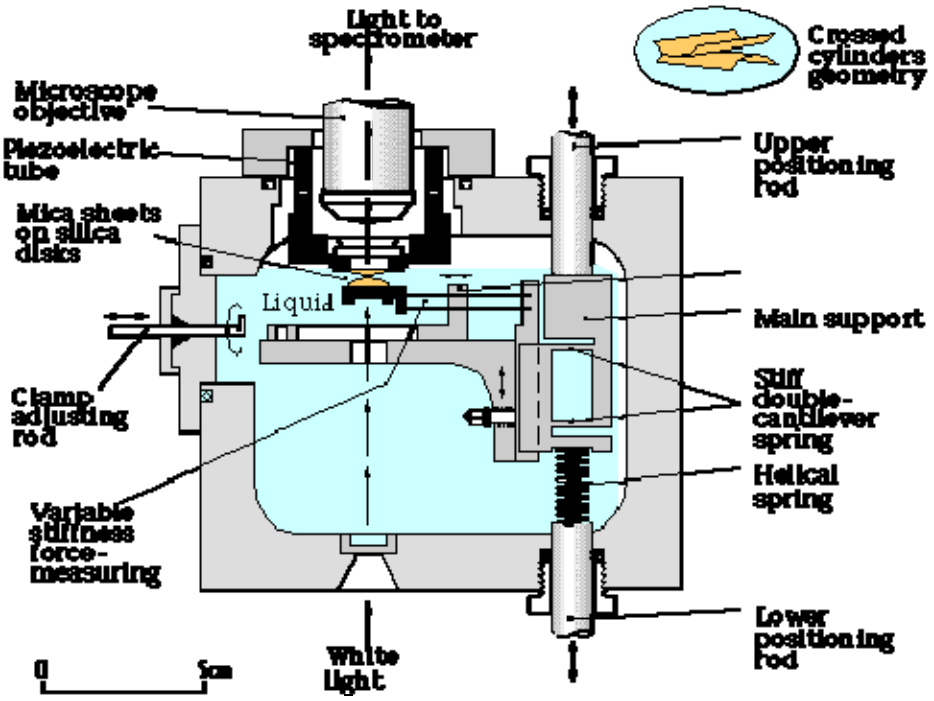

Figure 1.1 A schematic diagram of SFA Mark Ⅱ[44]

1.4 Drawbacks of current studies

There have been plethora of studies focused on domain formation of coexistence of phases (especially coexistence of L_d and L_o phases) and lipid rafts have received enormous attention and rekindled the interest in understanding the formation of domains in model membranes.[45-48] Lateral heterogeneities within model membranes have been broadly applied in understanding lipid domain formation and as analogues for lipid rafts.[49, 50] However, few studies directly characterize the interaction forces between membranes; and no studies have measured the interaction between solid-fluid phase separated membrane systems. For example, membrane phase separation has been found to greatly enhance membrane adhesion between vesicles which was hypothesized to be due to meta-fused states.[25, 38, 51] On the other hand, hydrophobic mismatch suggests that some adaptations will be made to such mismatch in order to avoid unfavorable exposure of hydrophobic surfaces to a hydrophilic environment.[52-54] Few studies have been focused on revealing the influence of hydrophobic mismatch caused by phase separation on membrane interactions. Instead, most studies have focused on characterizing phase diagrams and domain morphology. For example, atomic force microscopy is one of the most widely used techniques to characterize supported membranes and in the case of phase separated membranes allows for measurements of domain height due to alterations in the packing and composition of the domains.[30] However it is challenging to measure membrane-membrane interactions by AFM due to difficulties in forming a membrane on AFM tips.[31, 32] Fluorescence microscopy enables phase separated membrane domain morphology and size as a function of surface pressure, composition

and temperature[33, 34] to be investigated.

In this work, the interaction forces between supported, phase separated membranes of saturated and unsaturated phospholipid mixtures with different compositions are directly measured by SFA. The interaction force profiles are corroborated with vesicle zeta potential measurements and AFM and FM measurements of membrane domain morphology to quantify how membrane domains and phase separation impact membrane-membrane interactions such as van dear Waals, electrostatic, and hydrophobic contributions.

Material and Methods

2.1 Chemicals

1, 2-dipalmitoyl-sn-glycero-3-phosphoethanolamine (DPPE, melting point T_M = 62 °C);

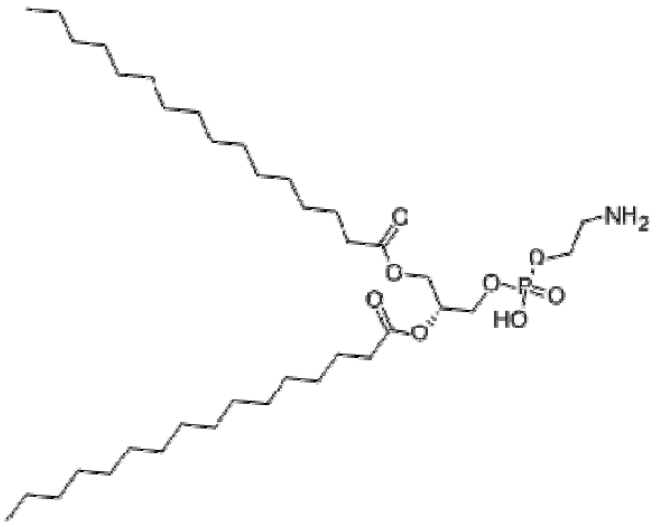

Fig. 2.1 Chemical structure of DPPE[55]

1, 2-dioleoyl-sn-glycero-3-phosphocholine (DOPC, melting point T_M = -20 °C).

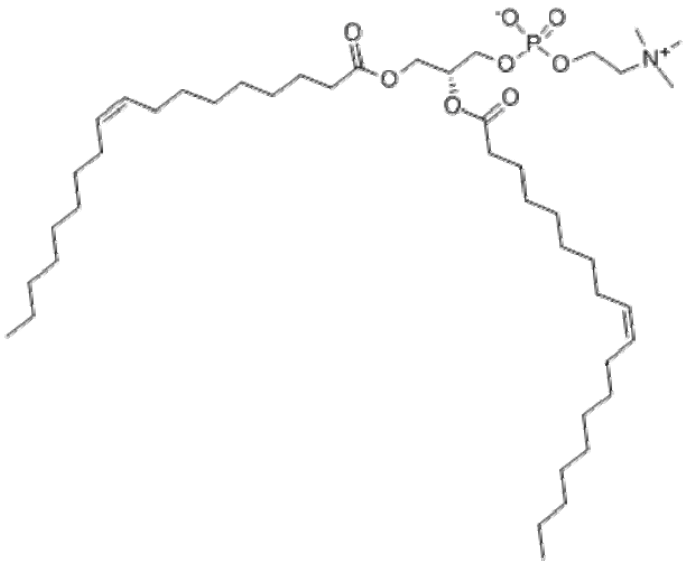

Fig. 2.2 Chemical structure of DOPC[55]

All lipids were purchased from Avanti Polar Lipids, Inc. (Alabaster, AL). N-(lyssamine Rhodamine B sulfonyl)-1, 2-dioloeoyl-sn-3-phosphatidylehanolamine (Rhod-DOPE) was purchased from Avanti Polar Lipids, Inc. (Alabaster, AL). Lipids were dissolved in chloroform at a concentration of 1 mg/mL. $NaNO_3$ 99.995% (Sigma, St. Louis, MO) was used as the monovalent salt in the electrolyte solutions. The water used was purified with a Milli-Q gradient water purification system with a resistivity of 18 MΩ• cm.

2.2 Sample Preparation

The mica-supported lipid bilayers were prepared by Langmuir-Blodgett (LB) deposition at room temperature using a Wilhelmy trough (Nima Coventry, U.K.). DPPE, as the inner layer, was deposited onto freshly cleaved mica by raising the substrates vertically through a compressed DPPE monolayer at the air-water interface with a surface pressure of 45 mN/m. The dipping speed was 1 mm/min. DPPE was found to form a strongly physisorbed monolayer on freshly cleaved mica, which minimizes molecular exchange between the two leaflets. The DPPE inner monolayer transfer ratio was 1.00 ± 0.02.[30]. The outer layer consisted of either 3:7 (mole %) or 1:1 mixture of DPPE: DOOC deposited onto DPPE monolayer on mica using LB deposition at 30 mN/m with a dipping speed of 4 mm/min. In order to decrease the possibility of oxidation of the unsaturated lipid, DOPC, the deposition process was completed within 30 min. The mixture outer layer transfer ratios were 0.89 ± 0.03 for 3:7 DPPE:DOPC outer layer, and 0.90 ± 0.02 for 1:1 DPPE:DOPC outer layer.

In some cases, monolayer was formed by vesicle fusion.[56] The procedures were previously described by J. Kurniawan *et al.*[30] Lipid mixtures were prepared in chloroform, dried under nitrogen, and then placed under vacuum for at least 4 h. Mixtures for fluorescence microscopy imaging contained 1 Rhod-DOPE. The dried lipids were hydrated with Milli-Q water to a concentration of 0.5 mg/mL, sonicated using a probe tip sonicator for 1 min, and then extruded through a 100 nm pore size polycarbonate membrane for 10 passes. Vesicle solutions for ZP were extruded and not probe tip sonicated to prevent titanium contamination. In some studies, a DPPE monolayer was incubated with the extruded vesicle solution for 1 h to create an asymmetric bilayer as in the Langmuir deposited case. In others, a freshly cleaved mica substrate was incubated with the vesicle solution to form the entire membrane by vesicle fusion. After incubation, excess vesicles were removed by extensively rinsing the sample with Milli-Q water.

However, as noted by J. Kurniawan[30], the formation of a uniform supported membrane using either vesicle fusion approach was problematic. High-resolution fluorescence microscopy and surface force measurements revealed the presence of tubules and tethered vesicles extending from the membrane surface rather than a uniform membrane. As a result, a significant repulsion was observed during the force measurements due to the confinement and compression of tubules and tethered vesicles between the supported membranes. In addition, the vesicle fusion method on either bare mica or a supported DPPE monolayer did not yield as complete

membranes as demonstrated by a greater number of defects in the membranes. Furthermore, membranes formed entirely by the vesicle fusion method on a bare mica substrate were of even lower quality in terms of uniformity and surface coverage compared to membranes formed by fusion to a DPPE monolayer. By using vesicle fusion to form the membrane, the fluorescence microscopy images demonstrated defects all over the membrane, compared to the outer layer using LB deposition, which yielded a reasonably well-packed membrane with fewer defects can be detected by FM images. As the membranes constructed using LB deposition were more uniform, all the results were carried on membranes formed by LB deposition in this work.

2.3 Zeta Potential Measurement (ZP)

The magnitude of the electrical charge of both membrane compositions was quantified by zeta potential measurement in 0.45 mM $NaNO_3$ solution at room temperature (Brookhaven Zeta Plus, Holtsville, NY). The solutions were extruded through 100 nm pore diameters polycarbonate Whatman membranes filter using Lipex Biomembrane extruder prior to the zeta potential measurements. Three independent experiments were carried out with ten measurements for each composition. The measured results showed that 1: 1 DPPE: DOPC (-16.75 ± 4.62 mV) had a higher surface potential than 3: 7 DPPE: DOPC (-10.28 ± 4.50 mV). It was in good agreement with results of electrostatic repulsion found from SFA experiments for both compositions.

2.4 Fluorescence Microscopy (FM)

FM images were obtained using a Nikon Eclipse E600 microscope connected to a CoolSNAP-Pro CCD camera at 20× and 40× magnification. Three independent samples were imaged for both compositions deposited on DPPE monolayer supported by mica at 30mN/m. FM images at water-air interface (without being deposited on DPPE monolayer) were obtained as well. Different domain morphologies and sizes were discovered for different compositions.

2.5 Atomic Force Microscopy (AFM)

AFM studies were obtained using an MFP3D-SA system (Asylum Research, Santa Barbara, CA). A silicon cantilever (model AC-240 Bruker, Santa Barbara, CA) with a spring constant of 1 N/m was used for imaging. A contact mode was used for all scans in Milli-Q gradient water. The average scan speed was 20 μm/s. The AFM images were analyzed using Gwyddion version 2.37.[57]

2D and 3D images were taken for both compositions to reveal the morphology of membrane surfaces and to measure the height differences between DPPE domains and DOPC region.

2.6 Surface Force Measurements (SFA)

As one of the most versatile and highest resolution technique in measuring membrane-

membrane interactions, SFA has been used extensively to measure the interaction forces between surfaces.[39-41] The mica substrates were coated with a 55-nm-thick evaporated silver layer on the back in order to produce fringes of equal chromatic order (FECO) by partially transmitting light directed normally through the surfaces. Back silvered mica was glued onto a glass cylinder as the solid support. After bilayers were deposited onto mica, the surfaces were transferred and mounted in the SFA under 0.5mM $NaNO_3$ solution. One of the surfaces was mounted on a fixed stage, while the other was mounted on a vertically displayable double-cantilever spring of a stiffness at 2.23×10^5 mN/m. The solution was saturated with the same lipid mixture as the outer layer to prevent lipid desorption from the substrates during the course of the measurements. After the surfaces were mounted, the SFA box was placed in a temperature-controlled room at room temperature for at least two hours for equilibration. A custom-automated SFA Mark Ⅱ was used for data collection. Observation of the position and displacement of FECO peak wavelengths within a spectrometer enables the measurement of the separation between surfaces which can be changed by constant and/or variable motor displacements via a computer-controlled motor system. A sensitive CCD camera (Princeton SPEC-10:2K Roper Scientific, Trenton, NJ) was interfaced with the spectrometer and computer data acquisition system to allow automated FECO wavelength determination. The membrane thickness was measured by the FECO wavelength shift from membrane contact relative to bare mica substrates after completing the experiment. Three independent SFA experiments for each composition were carried out and consistent results were obtained among the three independent experiments.

Results

3.1 Isotherm of outer layer mixtures

By using LB deposition and keeping the temperature at constant, room temperature, isotherm data can be obtained. Based on these isotherms, we could possibly calculate the thickness of different lipids, and then obtain the height different between these two kinds of lipids in mixture theoretically. The anhydrous outer monolayer thickness (T) was calculated from the known volumes occupied by the hydrocarbon chains and PE and/or PC headgroups given by

$$T = \frac{\left(2V_{hc} + V_{head}\right)}{A} \qquad \text{(Eq.5)}$$

where $V_{hc} = (27.4 + 26.9n)$ Å^3 is the average volume of a saturated n-carbon chain in the gel state and Å^3 $V_{hc} = (27.4 + 26.9n + 2 \times 20.5)$ is the average volume of an unsaturated n-carbon chain with one double-bone in the liquid state. $V_{head} = 324.5$ Å^3 is the average head group volume of PC; $V_{head} = 243$ Å^3 is the average head group volume of PE[58]. A is the deposited area per lipid, which can be obtained from the isotherm plots.

Thus, we are able to calculate the volume of each DPPE and/or DOPC molecule without any other information, just based on Equation.5 and parameters listed above.

$$\begin{aligned} V_{DPPE} &= 2V_{hc} + V_{head} \\ &= 2 \times (27.4 + 26.9 \times 15) + 243 \\ &= 1104.8\ \mathring{A}^3 \end{aligned} \qquad \text{(Eq.6)}$$

$$V_{DOPC} = 2V_{hc} + V_{head}$$
$$= 2 \times (27.4 + 26.9 \times 15 + 2 \times 20.5) + 324.5 \quad \text{(Eq.7)}$$
$$= 1268.3\ \mathring{A}^3$$

Using Equation.5-7 and combining the Area per molecule (A value in Equation.5) read from isotherm plots, thickness of both DPPE and DOPC in mixture can be obtained.

3.1.1 Isotherm of 1:1 DPPE:DOPC mixture

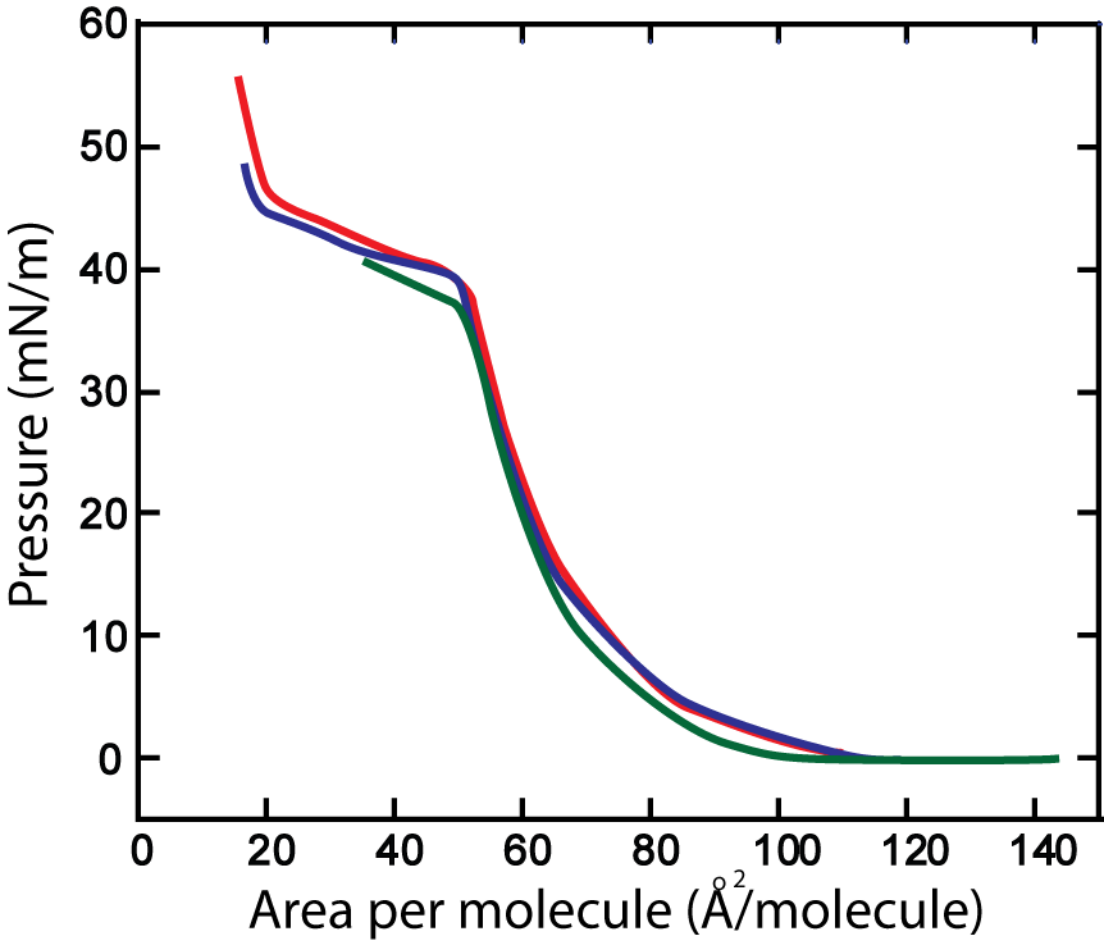

Figure 3.1 Isotherms of 1:1 DPPE:DOPC mixture at room temperature

Three sets of independent experimental data were collected and plotted as shown in Figure 3.1 for 1:1 DPPE:DOPC mixture. Consistent results were obtained indicating these data were reliable and reproducible. Especially, data at the pressure we are interested (30 mN/m) were nearly perfectly consistent with each other.

Area per molecule at pressure of 30 mN/m is 54.7 ± 0.2 $Å^2$ / molecule. Since DPPE was in solid phase and saturated (would not be oxidized with longer exposure time), we assumed that DPPE molecules had the same area per molecule in the mixture as in pure DPPE, i.e. ~43.0 $Å^2$/molecule at 30 mN/m, which was obtained from pure DPPE isotherm and was shown in Fig.3.3. We also assumed that the area fraction that each lipid molecule occupied was based on the ratio of their amounts in the mixture. Thus, we calculated the DOPC area/molecule at 30 mN/m using the following relationship,

$$Area/molecure_{mixture} = 50\% Area/molecure_{DPPE} + 50\% Area/molecure_{DOPC} \quad \text{(Eq. 8)}$$

$$54.7 = 0.5 \times 43.0 + 0.5 \times Area/molecure_{DOPC}$$

$$Area/molecure_{DOPC} = 66.4\ A^2 / \text{molecule}$$

Thus the thickness of DOPC lipid molecule in 1:1 DPPE:DOPC mixture is,

$$T_{DOPC} = \frac{V_{DOPC}}{A_{DOPC}} = \frac{1268.3}{66.4}$$
$$= 19.1Å \approx 1.9nm$$

and the thickness of DPPE lipid molecule is,

$$T_{DPPE} = \frac{V_{DPPE}}{A_{DPPE}} = \frac{1104.8}{43.0}$$

$$= 25.6\text{Å} \approx 2.6nm$$

3.1.2 Isotherm of 3:7 DPPE:DOPC mixture

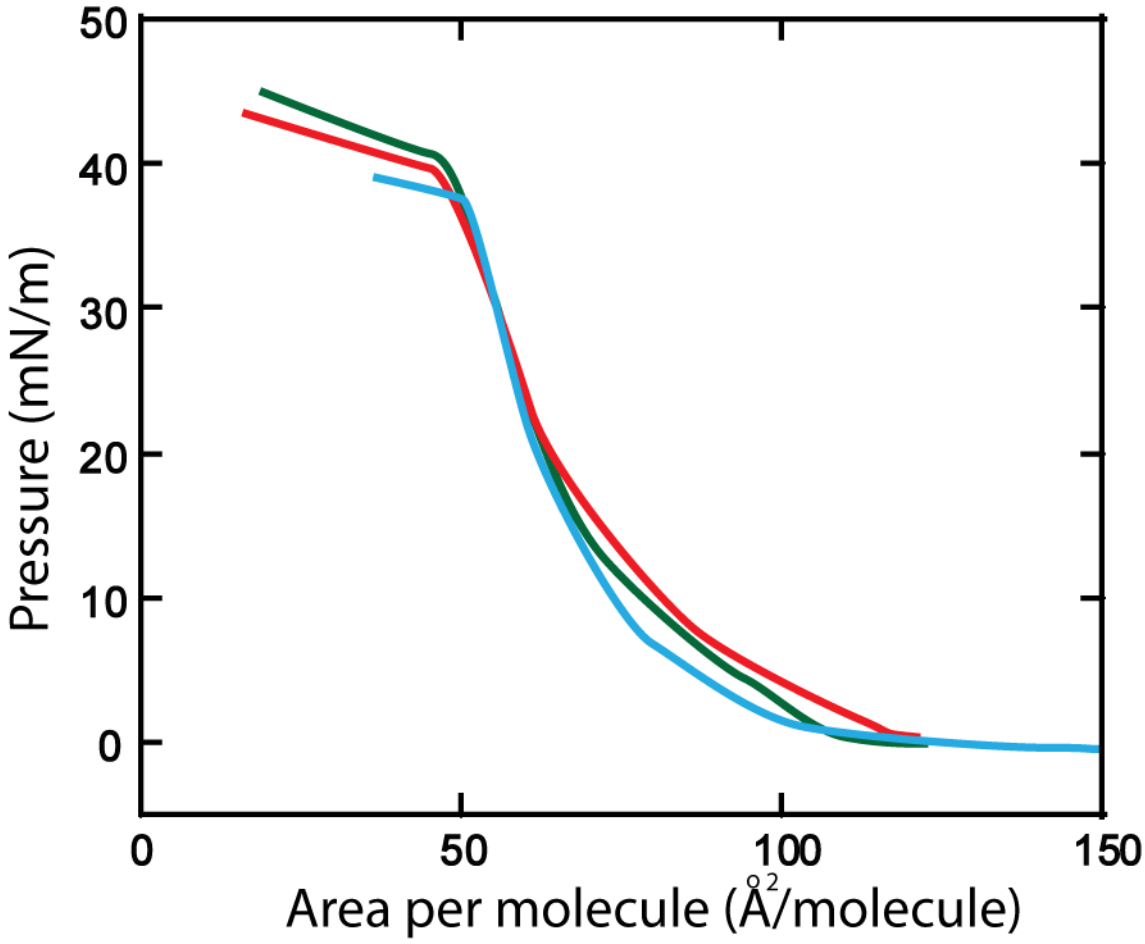

Figure 3.2 Isotherms of 3:7 DPPE:DOPC mixture at room temperature

Three sets of independent experimental data were collected and plotted as shown in Figure 3.2 for 3:7 DPPE:DOPC mixture. Consistent results were acquired within pressure around 30 mN/m which was the target pressure deposited onto inner

monolayer. Area per molecule for this mixture at pressure of 30 mN/m is 56.3 ± 0.3 $Å^2$ / molecule.

Keeping the same assumptions above and calculating the area per molecule of DOPC in this mixture is,

$$Area/molecure_{mixture} = 30\% Area/molecure_{DPPE} + 70\% Area/molecure_{DOPC} \quad \text{(Eq. 9)}$$

$$56.3 = 0.3 \times 43.0 + 0.7 \times Area/molecure_{DOPC}$$

$$Area/molecure_{DOPC} = 62.0\ A^2 / \text{molecul}$$

Therefore the thickness of DOPC in 3:7 DPPE:DOPC mixture is,

$$T_{DOPC} = \frac{V_{DOPC}}{A_{DOPC}} = \frac{1268.3}{62.0}$$
$$= 20.4A \approx 2.0nm$$

Compared with the thickness of DOPC obtained from 1:1 DPPE:DOPC mixture (1.9 nm), the results were in good agreement within error. Since we were assuming the DPPE molecules were not changing with exposure time, and thus not changing with the environment with surroundings (different ratios of DOPC), the thickness of DPPE was supposed to be the same as what we obtained from 1:1 DPPE:DOPC mixture (2.6 nm).

3.1.3 Height difference between DPPE and DOPC molecule from isotherm

Next, we compare the results of 1:1 DPPE:DOPC and 3:7 DPPE:DOPC with the pure DPPE and DOPC in isotherm.

Isotherm plots of the lipid mixtures used to make the outer monolayer of the membrane bilayer at room temperature were obtained as shown in Figure 3.3. The isotherms in between pure DPPE isotherm (left one) and pure DOPC isotherm (right one) were in good agreement based on the ratio of lipid mixtures with pure isotherms, i.e. 1:1 DPPE:DOPC isotherm was ~50% pure DPPE + 50% pure DOPC under 35mN/m within errors. With pressure going up to the collapse of DOPC, the mixture isotherms showed more features of DPPE isotherm.

Thus, we calculated the DOPC area/molecule at 30 mN/m to be 66.4 $Å^2$/molecule for 1:1 DPPE:DOPC and 62.0 $Å^2$/molecule for 3:7 DPPE:DOPC. Furthermore, we calculated the thickness of both lipids in mixture, 2.6 nm for DPPE and 1.9-2.0 nm for DOPC, indicating the height difference between these two kinds of lipids were ~0.7 nm. We will discuss about the height difference between these two lipid molecules using AFM images in the following section and interestingly quite different results were obtained.

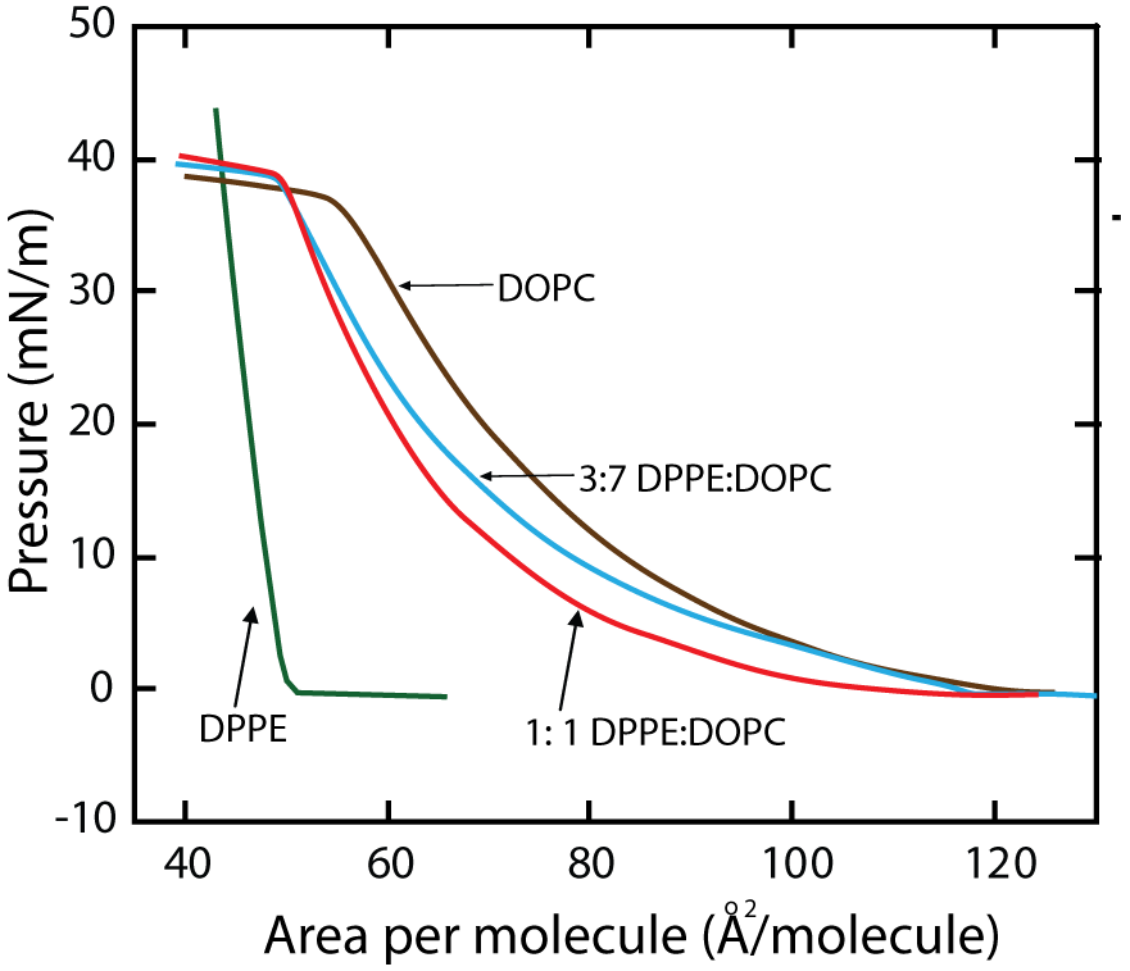

Figure 3.3 Isotherms of DPPE, 1:1 DPPE:DOPC, 3:7 DPPE:DOPC, DOPC at room temperature.

Both compositions showed partial properties of pure DPPE and DOPC in isotherm plot. However, the value of area per molecule of the mixed lipids membrane did not follow strictly with their ratios of each composition, which suggested that the mixing of these two components was non-ideal mixing.

3.2 AFM scans of outer layer domains

AFM scans gave the information about the membrane deposited on DPPE inner monolayer, unlike isotherm plots obtained using LB deposition and FM images acquired from water-air interface. Therefore, membranes used for AFM scans were more closed to the membranes in cell and the membranes used for SFA experiments.

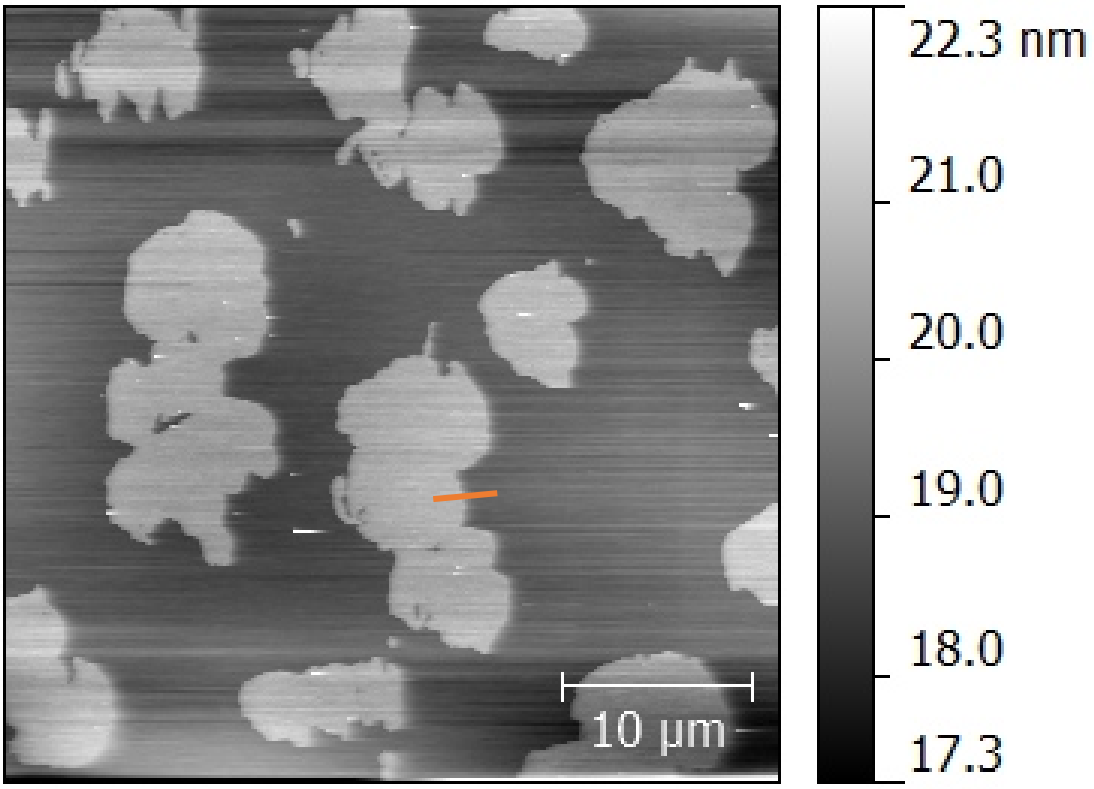

3.2.1 AFM scans of 1:1 DPPE:DOPC outer layers

Figure 3.4 A representative 40 µm × 40 µm AFM image of 1:1 DPPE:DOPC.

Figure 3.4 showed a representative 40 μm × 40 μm AFM image of 1:1 DPPE:DOPC deposited on DPPE monolayer supported by mica in 0.45 mM $NaNO_3$ solution. The bright shapes were solid-phase DPPE domains with a dimension of 12 ± 3 μm × 15 ± 5 μm. The dark area was mainly fluid-phase DOPC region with little DPPE in it. The shapes of DPPE domains were jagged in shape, which was in good agreement with FM images discussed below. Only very little DPPE was mixed in DOPC region which can be verified by calculating the area fraction of the DPPE domain in the overall area. By doing that, we obtained the area fraction of DPPE in the overall area was 46.6% ± 1.5%. Compared to the original molar fraction of DPPE in the membrane, which was 50%, we could get that only ~3% of DPPE was in DOPC region based on data obtained from three independent AFM scans. We believed that the reason why ~3% of DPPE did not give bright spot in dark DOPC region was this small amount of DPPE was beyond the AFM resolution to image.

Moreover, height variation information was shown in AFM scans. We are mainly interested in the height difference between DPPE domain and DOPC region. By acquiring the height difference using AFM scans, we could possibly compare the results with the height difference that we obtained from isotherm figures previously.

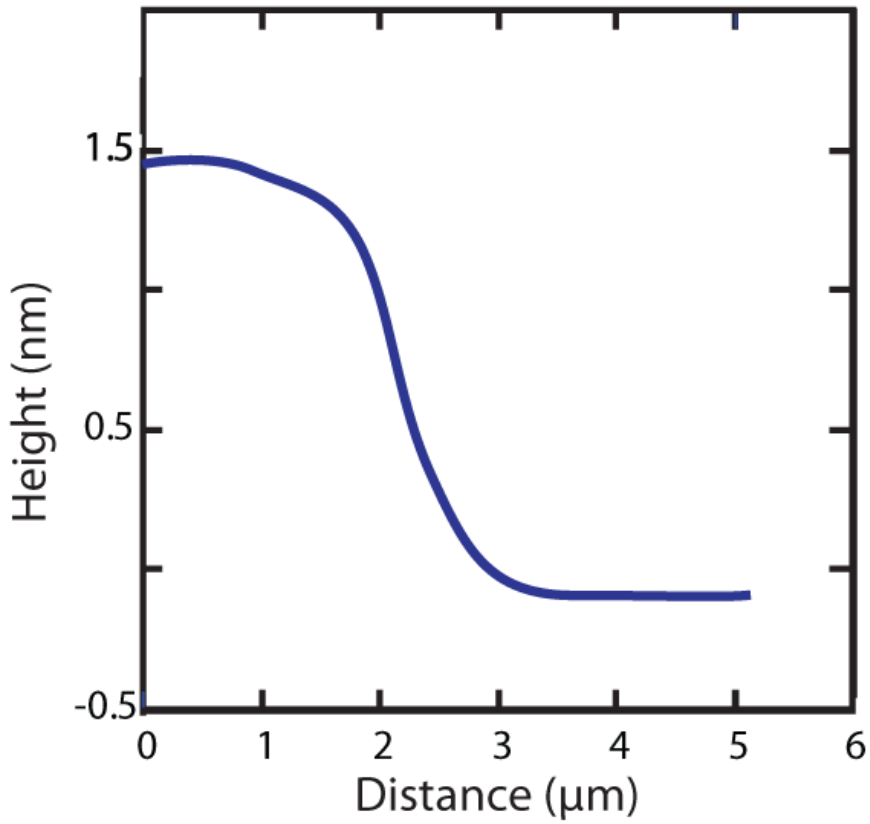

Figure 3.5 Corresponding cursor profile as indicated (orange bar) in Figure 3.4 to obtain height profile.

A representative height profile shown in Figure 3.5 obtained at the position shown in Figure 3.4 by an orange bar. An average height difference of 1.5 ± 0.3 nm between DPPE domains and DOPC regions were acquired from AFM images. This was much larger than the height difference calculated from isotherm above (~0.7nm).

We attribute the height differences to different mechanisms of forming the domain morphology. We will discuss this later in discussion session.

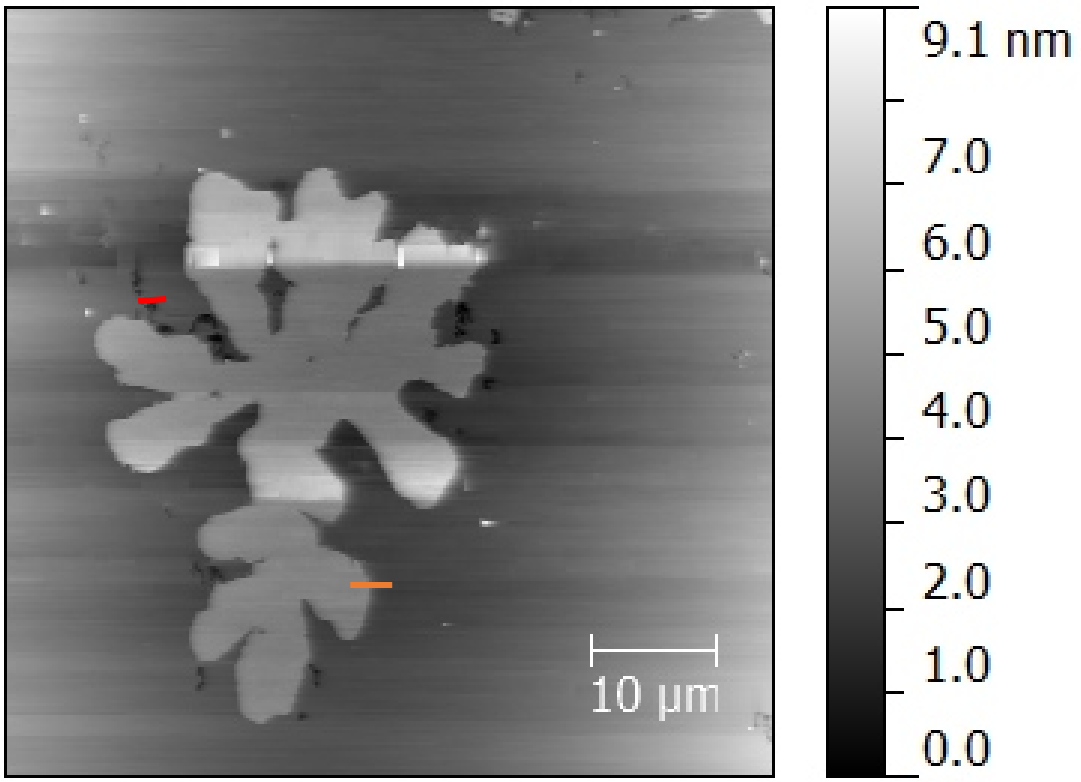

3.2.2 AFM scans of 3:7 DPPE:DOPC outer layers

Figure 3.6 A representative 60 µm × 60 µm AFM image of 3:7 DPPE:DOPC.

3:7 DPPE:DOPC composition shows different domain morphologies in AFM scans. Figure 3.6 displays a 60 µm × 60 µm AFM image with the dimension of DPPE domain being 30 ± 5 µm × 40 ± 8 µm. Compared to the size and shape of domains in 1:1 DPPE:DOPC mixture, 3:7 DPPE:DOPC domains were bigger and more separated. The average size of domains was four times as in 1:1 DPPE:DOPC and the average distance between domains was more than twice as it in 1:1 composition.

The area fraction analysis demonstrates similar results as 1:1 composition. DPPE domains were found to be 21.0% ± 2.2% of the overall area. The reason why the area fraction analysis results in less DPPE in the domain was that within the resolution of AFM scans, we could only get 1-3 DPPE domains of 3:7 DPPE:DOPC in one AFM scan. As the DPPE domain size was much bigger in 3:7 mixture than in 1:1 mixture, the area fraction analysis of 3:7 compositions was believed less accurate than that of 1:1 composition.

Only a few of defects were observed in 3:7 DPPE:DOPC AFM images (indicated as the red bar in Figure 2C) and there was no defects observed within the AFM resolution in 1:1 DPPE:DOPC. The averaged depth of defects was 2.0 ± 0.2 nm (7 measurements in 3:7 AFM images only), which is in good agreement with calculated DPPE/DOPC thickness from isotherms (2.3nm and 1.9nm, respectively).

A representative height difference profile was shown in Figure 3.7 at the position indicated in orange bar in Figure 3.6. The height difference between DPPE domain and DOPC region was 1.6 ± 0.3 nm, which is in good agreement with 1:1 DPPE:DOPC result (1.5 ± 0.3 nm).

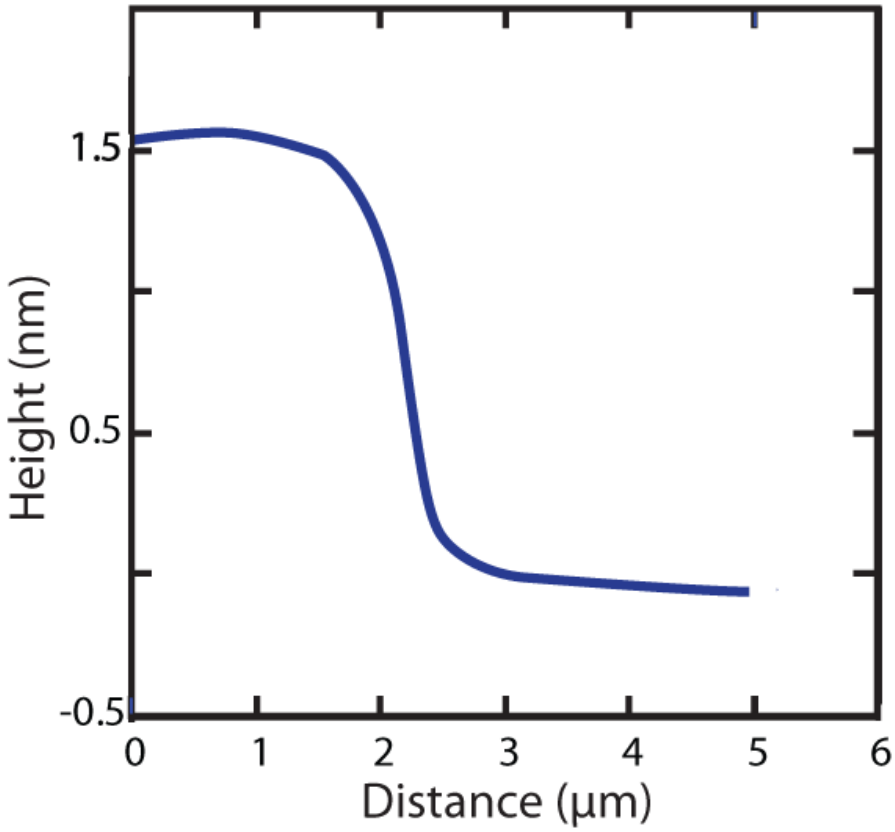

Figure 3.7 Corresponding cursor profile as indicated (orange bar) in Figure 3.6 to obtain height profile.

Besides the height difference, we found more interestingly that the height difference "vanishes" in the order of micrometer which gave a large "buffer zone" as a transition region between DPPE domains and DOPC region. It might be the scan speed of AFM was fast that caused the delay in response of height variation. Further slow scans will be done to deeply investigate this phenomenon.

A 3-D image (Figure 3.8) was obtained at the same position shown in Figure 3.6 to display the morphology and height difference between gel phase domains and fluid phase region.

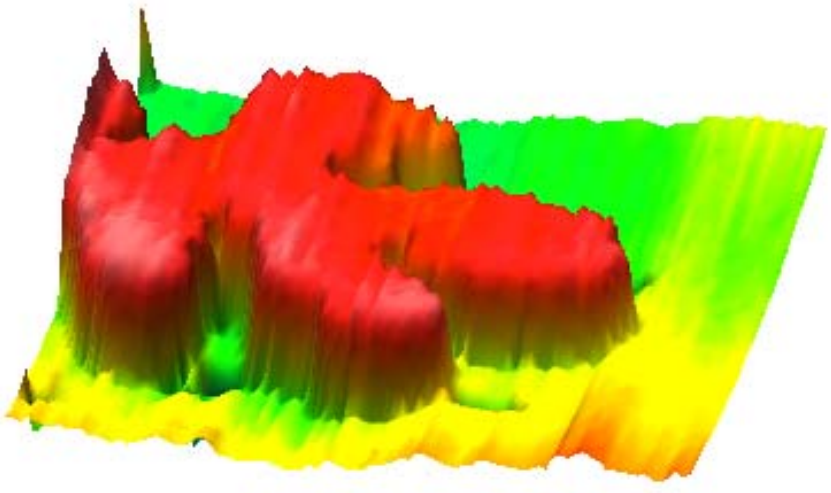

Figure 3.8 3-D image of DPPE domain and DOPC region

3.3 Fluorescence microscopy of outer layers

FM images showed similar domain shape and size of both 1:1 and 3:7 DPPE:DOPC membrane as in AFM scans. Different from AFM, FM images were obtained at water-air interface and as dye was used in FM experiments to distinguish DPPE and DOPC, the dark region was DPPE and bright region was DOPC, conversely to the AFM scans.

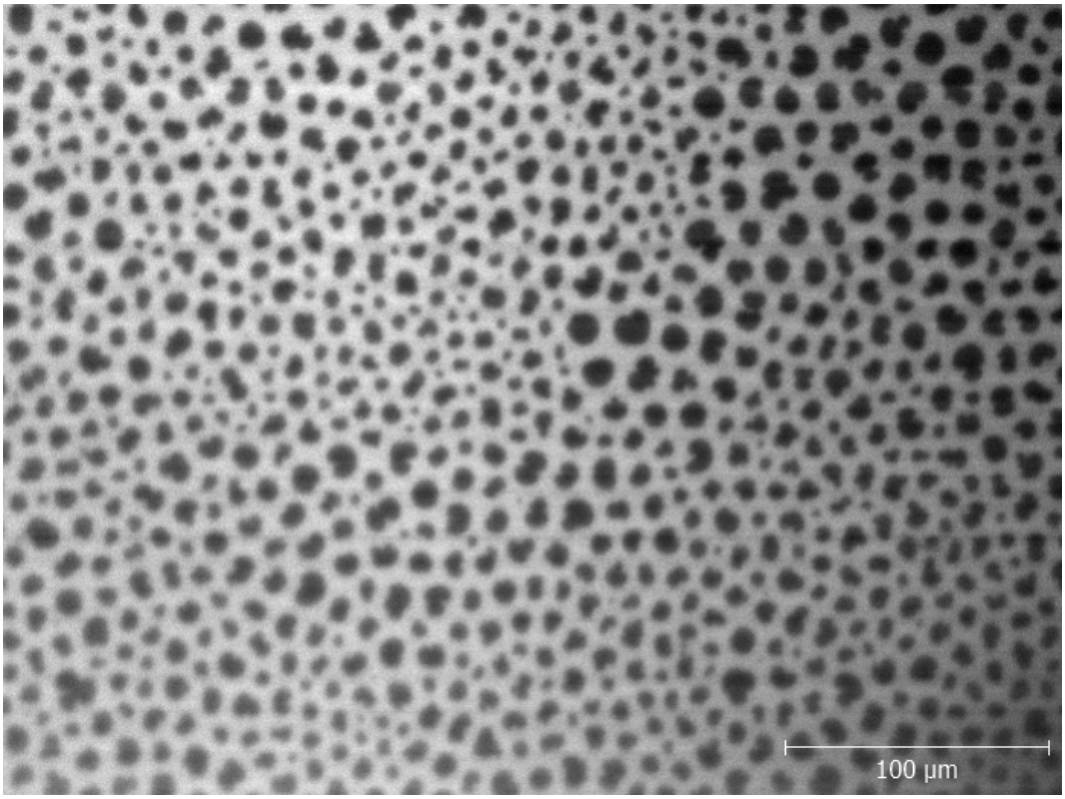

Figure 3.9 FM image of 1:1 DPPE:DOPC mixture at 30 mN/m at water-air interface at 20X magnification

A 400 µm × 300 µm FM image of 1:1 DPPE:DOPC deposited on DPPE monolayer supported by mica was shown in Figure 3.9. Round-shape domains were found in 1:1 DPPE:DOPC mixture in FM experiments. The average dimension of domain size was $11\times 15\ \mu m^2 \pm 4 \times 7\ \mu m^2$ and the area fraction analysis gave the result of 44.7% ± 2.0% DPPE in dark region.

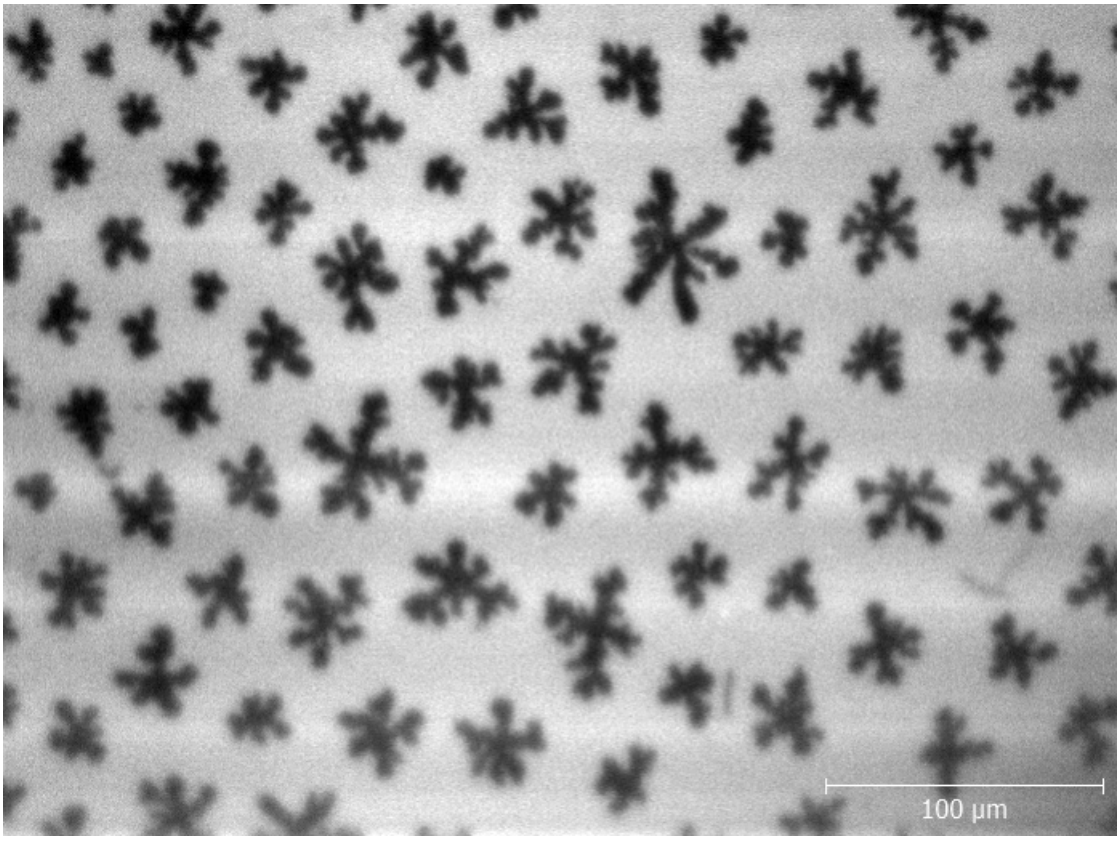

Figure 3.10 FM image of 3:7 DPPE:DOPC mixture at 30 mN/m at water-air interface at 20X magnification

The FM image of 3:7 composition outer layer also showed the flower-shaped DPPE domain with the dimension of 26 ± 4 µm × 37 ± 5 µm. The area fraction analysis demonstrates similar results as obtained from AFM scans. 24.1% ± 1.2 % of area was found in DPPE domains, which was believed to be more accurate than the AFM results since larger area was scanned in FM than AFM, resulting in more domains in the scanned area.

As the surface pressure was able to be controlled while imaging on FM, we could possibly obtain the domain size and shape as a function of surface pressure.

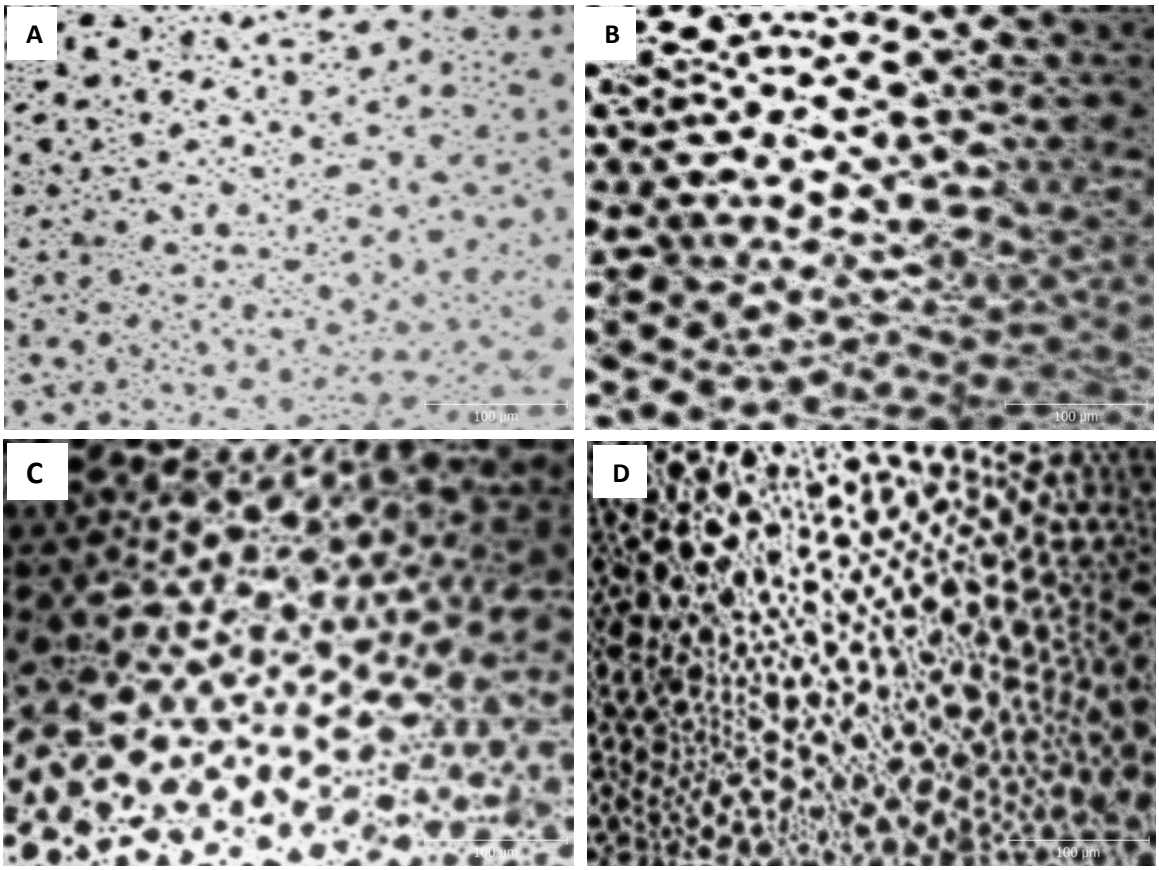

Figure 3.11 FM images of 1:1 DPPE:DOPC at the pressure of (A) 10 mN/m, (B) 15 mN/m, (C) 30 mN/m, (D) 35 mN/m at 20X magnification.

Figure 3.11 demonstrated domain size and shape of 1:1 DPPE:DOPC changed very little with increasing pressure after 15 mN/m. The same feature was found in 3:7 DPPE:DOPC. The increasing pressure only changed the density of domains while shape and size of them maintained. This indicated that the domain size and shape do not depend on the pressure exerted at the surface and Figure 3.11 showed that they are not as a function of time either.

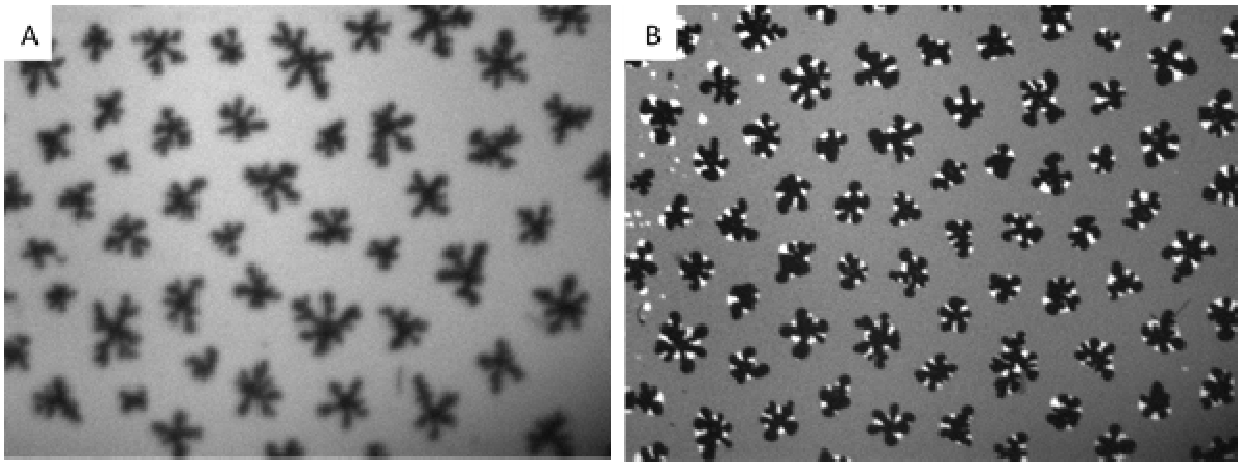

Figure 3.12 FM images of 3:7 DPPE:DOPC at the pressure of 30 mN/m after (A) 30 min, (B) 120 min at 20X magnification.

The FM images of 3:7 DPPE:DOPC showed that the domain size and morphology almost remained the same 30 min and 120 min after reaching the targeted pressure (30 mN/m). However, some degradation was found around the DPPE domains shown in Figure 3.12 (B) as bright spots. They were believed to be the degradation of unsaturated lipid, DOPC in this case, after long time exposure in oxygen containing condition. Similar results were obtained in 1:1 DPPE:DOPC mixture (not shown here). It is interesting to discover that the degradation mainly happened around DPPE domains and this will be discussed later in discussion section.

3.4 SFA measurements of both compositions as outer layer membrane

SFA experiments provides force measurements versus distance between opposing surfaces, *i.e.* force-distance profile, F(D). Results obtained from SFA experiments revealed the membrane thickness as well. Thickness of a single monolayer including hydration layer can be measured. Before further discuss the results of the measured F(D) profile, it is crucial to establish a method to describe the thickness of bilayers, which we are primarily interested in. The F(D) profile is based on the contact FECO wavelength after removal of the deposited outer layer at the end of the experiments, i.e. D = 0 was set at the top of DPPE inner monolayer.

By comparison, it's useful to acquire the thickness of theoretical anhydrous layer. Using Equation 5-8, and combining the results from isotherm plots, we can calculate the theoretical thickness of anhydrous mixed lipid membrane. For example, the thickness of anhydrous outer 1:1 DPPE:DOPC monolayers deposited at A = 54.7 $Å^2$ per molecule (π = 30 mN/m) is

$$T = \frac{50\%V_{DPPE} + 50\%V_{DOPC}}{A} = 21.1\,Å$$

3.4.1 SFA of 1:1 DPPE:DOPC mixture as outer layer membrane

Figure 3.13 showed three independent measured force-distance, F(D), profiles between opposing membranes with 1:1 DPPE:DOPC as the outer layer in 0.5 mM $NaNO_3$ solution. Results displayed great consistency. The thickness of a single outer

1:1 DPPE:DOPC monolayer including hydration layer is ~32.6 ± 1.3 Å. This is reasonably greater compared to theoretically calculated anhydrous outer layer (21.1Å).

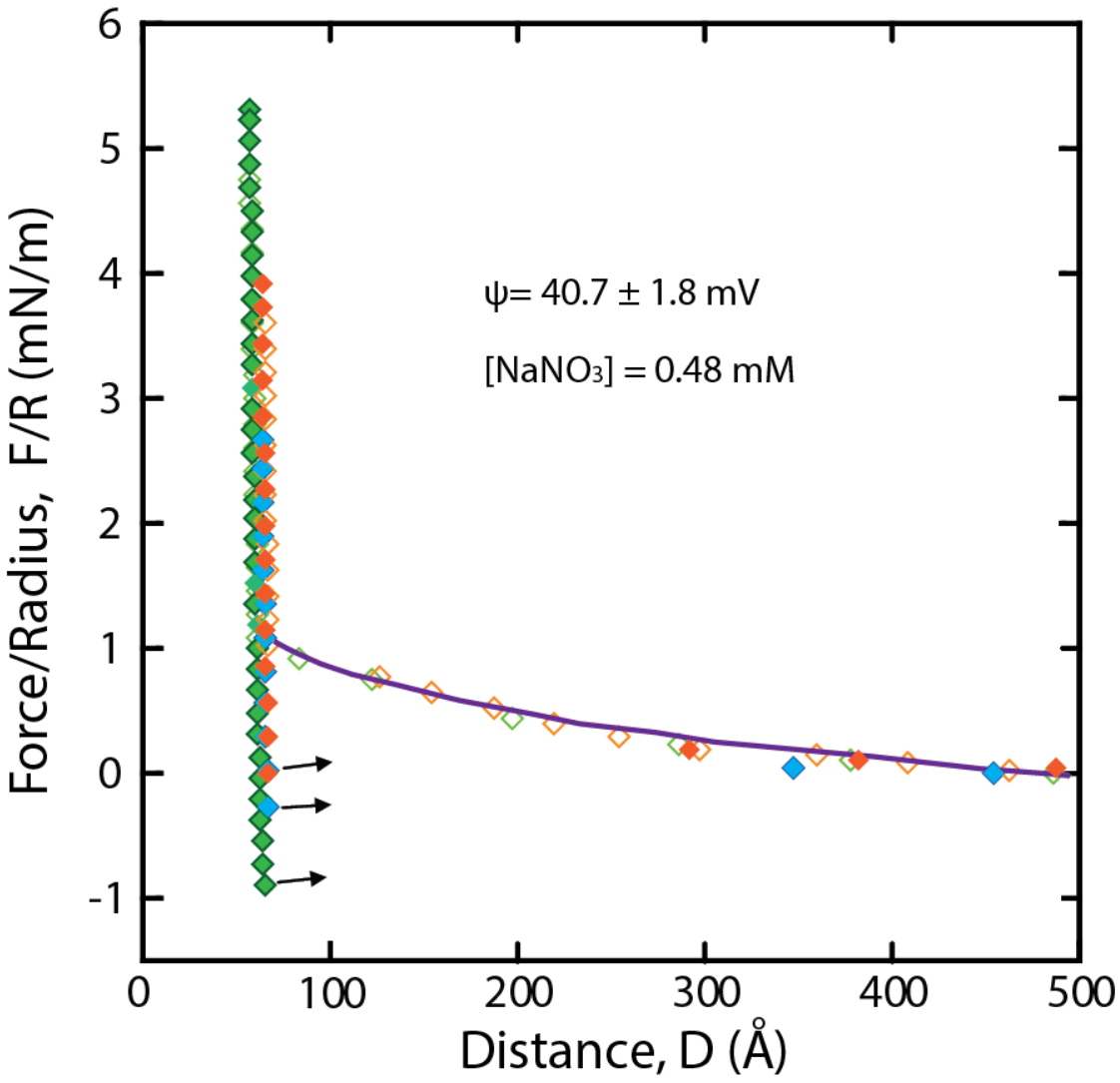

Figure 3.13 Force-distance profiles between 1:1 DPPE:DOPC membranes in 0.5mM $NaNO_3$ solution. D = 0 is defined as contact between the inner DPPE monolayers (△ : approach ; ◆ : separation). The solid line is the electrostatic contribution with the origin of charge at the membrane interface.

The thickness of the bilayer was assumed to remain constant during the experiments. This is reasonable given that DPPE (T_{mp} = 65 ℃) and DOPC (T_{mp} = -20 ℃) were deposited at room temperature and no phase changes or density changes are expected to take place.

The arrows in Figure 3 is the predicted van der Walls interaction $F = (-AR)/(6D^2)$ with a Hamaker constant of A = 7×10^{-21} J.[38, 59] Upon separation of the membranes, a substantial adhesion was measured, where the van der Waal's plane was located at 73.8 Å from D = 0, which is 7.6 Å from bilayer contact. The magnitude of the adhesion was 2.4±0.3 mN/m for 1:1 DPPE:DOPC membranes as shown in Figure 3.12. when the repulsive electrostatic contribution is accounted for, approximately 0.4 mN/m greater than the vdWs prediction.

Figure 3.14 demonstrated the Force-Distance data on a semilogarithmic plot in order to find out the source of the weak repulsive contribution to the force profile. The Poisson-Boltzmann (P-B) equation was used to fit the electrostatic contribution to the force profile. Assuming the origin of charge was at DPPE-DPPE inner monolayer, the best electrostatic fit was acquired for a salt concentration of 0.48 mM with a surface charge of 2.3 ± 0.1 mC/m^2 or a surface potential of 40.7 ± 1.8 mV. As shown in the semilog plot, the decay length of the repulsion is given by the electrolyte concentration of 0.48 mM $NaNO_3$ or $\kappa^{-1} \sim 14$ nm. Since the electrolyte concentration in the solution was 0.5 mM $NaNO_3$ which was higher than the concentration

calculated by the Debye length (0.48 mM), this indicates the repulsive force is electrostatic. Considering the headgroups of PC and PE lipids are zwitterionic and neutral in charge at pH 6, thus the overall membrane should be neutral, an electrostatic repulsion was unexpected. However, there have been reports on revealing why this electrostatic repulsion exits in neutral system.[30, 60, 61] Hemmerle, A. *et al*, discovered that some unsaturated lipids were charged due to contamination. Kurniawan, J. observed both saturated and unsaturated lipids were negatively charged via zeta-potential measurement.

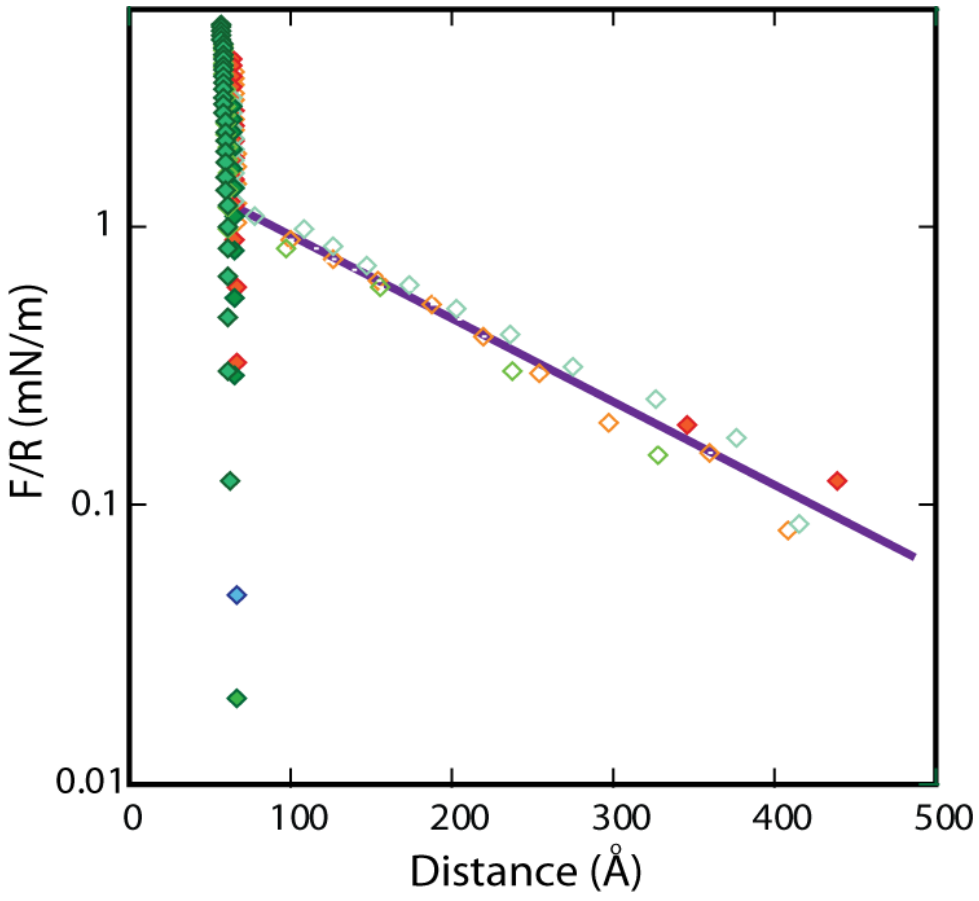

Figure 3.14 Semilogarithmic plot of Figure 3.12 and fit of electrostatic contribution.

3.4.2 SFA of 3:7 DPPE:DOPC mixture as outer layer membrane

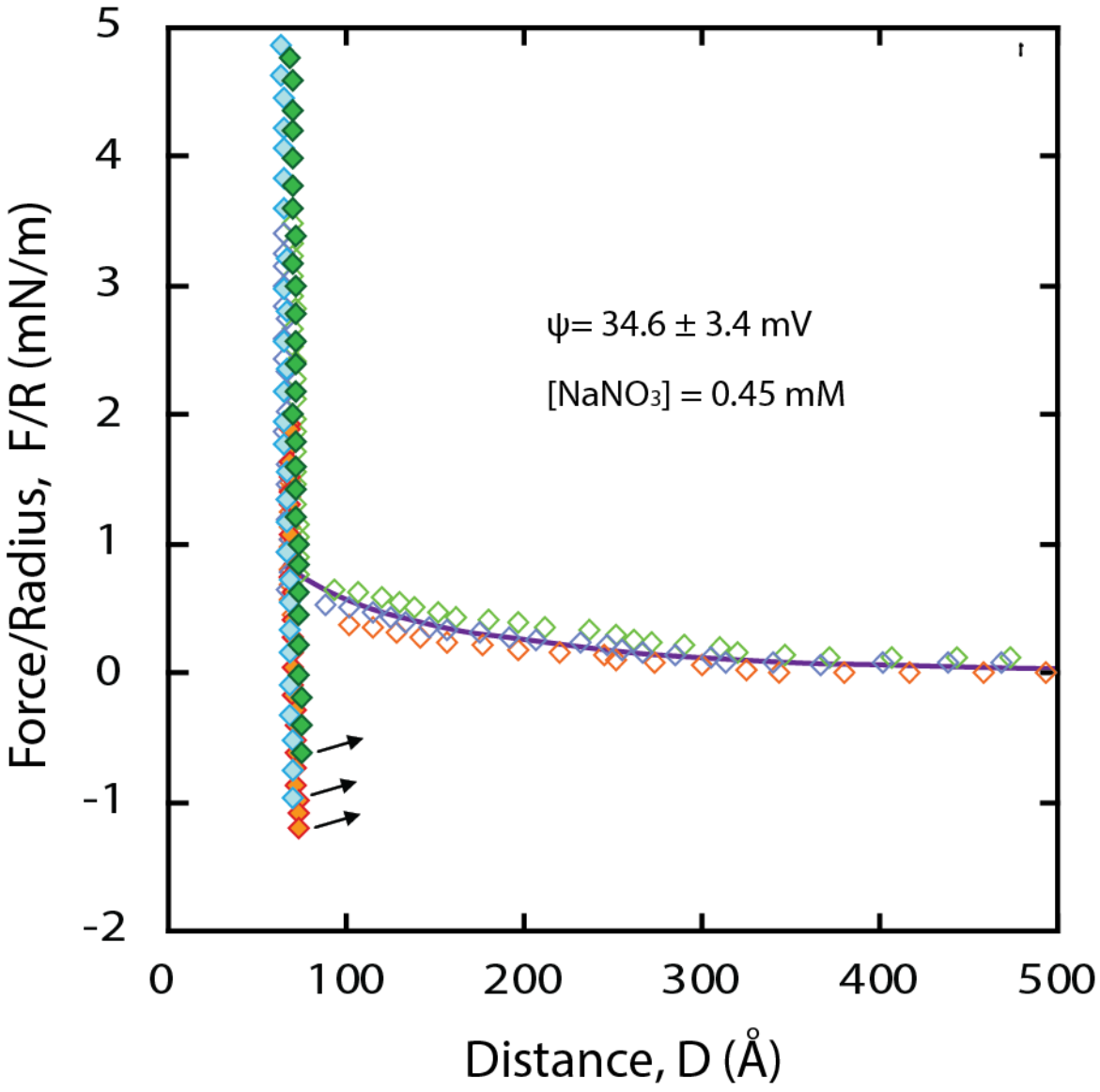

Figure 3.15 Force-distance profiles between 3:7 DPPE:DOPC membranes in 0.5mM $NaNO_3$ solution. D = 0 is defined as contact between the inner DPPE monolayers (◇ : approach ; ◆ : separation). The solid line is the electrostatic contribution with the origin of charge at the membrane interface.

Figure 3.15 shows the measured F(D) profile between opposing membranes with 3:7 DPPE:DOPC as the outer layer in 0.5 mM $NaNO_3$ solution. The F(D) plot was based on DPPE-DPPE inner monolayer contact (D = 0). The thickness of a single hydrated outer 3:7 DPPE:DOPC monolayer is ~34.3± 1.6 Å, greater than the calculated anhydrous 3:7 DPPE:DOPC monolayer (21.5 Å).

The magnitude of adhesion is ~2.2 ± 0.2 mN/m, comparable to the predicted vdW attraction (2.0 mN/m) with the vdW plane at D = 76.2 Å, which is 7.6 Å from bilayer contact. The electrostatic was fitted by P-B equation and was obtained for a salt solution of 0.45 mM with a surface charge of 2.5 ± 0.2 mC/m^2 or a surface potential of 43.6 ± 1.1 mV. In the case of 3:7 DPPE:DOPC outer layer, a weaker electrostatic was acquired which was in agreement with the zeta potential measurement discussed below.

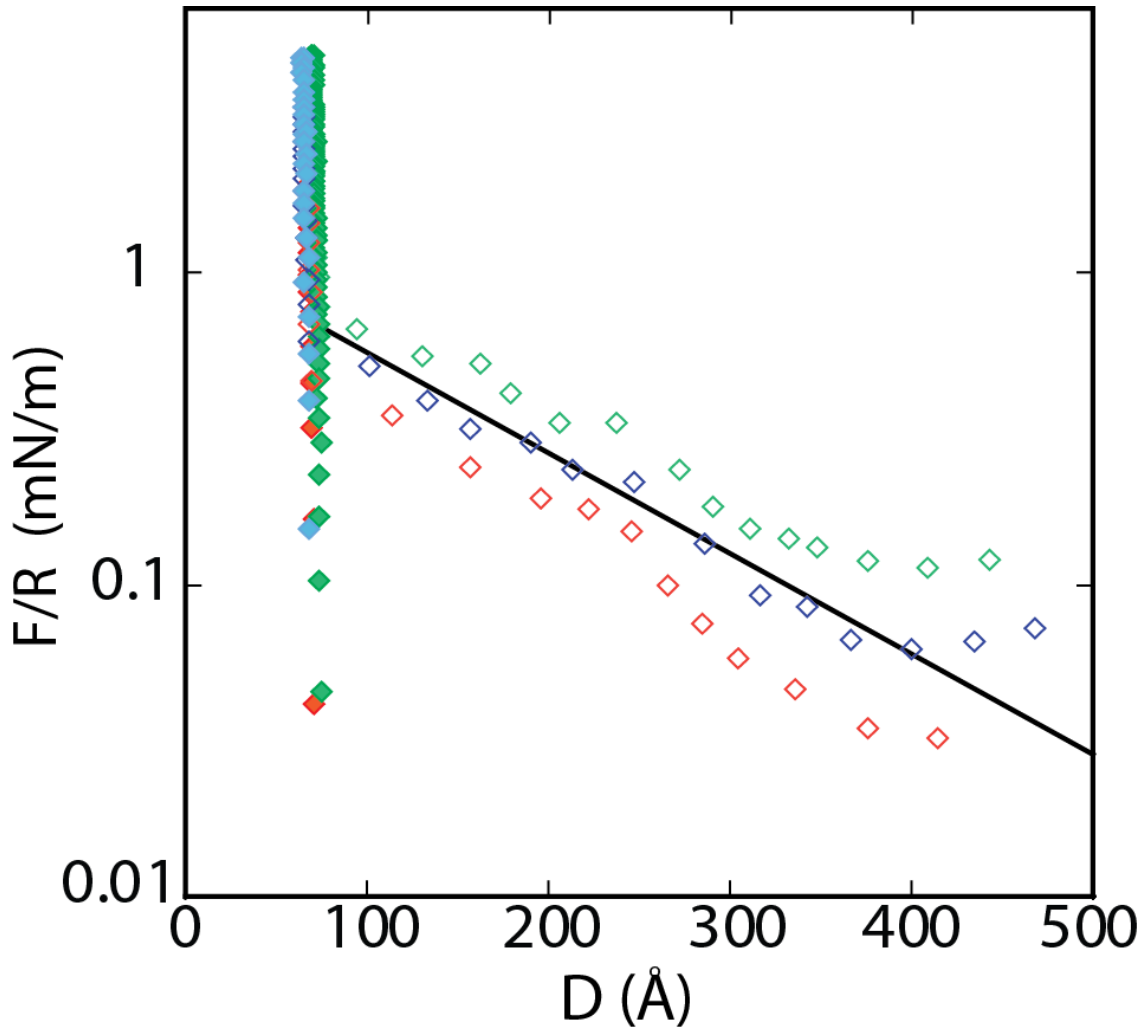

Figure 3.16 Semilogarithmic plot of Figure 3.14 and fit of electrostatic contribution.

Discussion

4.1Adhesion and Electrostatic Repulsion

In both cases, similar interaction force-distance profiles of these two compositions were found. A predominantly short-range vdWs attraction with a weak long-range electrostatic repulsion was measured. First we discuss adhesion. It has been considered adhesion between lipid membranes includes van der Waals and hydration interactions. As detailed above in result section, adhesion between 1:1 DPPE:DOPC membranes was ~2.4 mN/m, and 3:7 DPPE:DOPC membranes was ~2.2 mN/m, which both were within the vdW predictions of pure PE-PE and PC-PC membranes. The variation in adhesion is not due to membrane restructuring, as no changes in membrane-membrane contact position or increase in adhesion with contact time were observed. In addition, the domains in the supported bilayers were stable over time as evidenced by FM and AFM imaging.[62] These findings suggest that the measured differences in adhesion in the three independent experiments are due to different ratios of solid (DPPE) phase and fluid (DOPC) regions in the two membranes and their orientation in the contact region (Inset of Figure 3B). A schematic of the different opposing membrane domain regions is shown in Figure 3B. To better quantify the adhesion, the repulsive electrostatic contribution was subtracted from the measured force profile. The remaining interaction profile is shown in Figure 3B. The lines are the predicted van der Waals attraction for contacting solid phase DPPE-DPPE (Hamaker constant, $A = 7.5 \times 10^{-21}$ J), solid phase DPPE interacting with fluid phase DOPC ($A \approx 7.2\times 10^{-21}$ J), and fluid phase DOPC-DOPC ($A = 6.9\times 10^{-21}$ J) where $F/R = -A/(6D^2)$ [38, 59]. As can be seen, the measured adhesion is consistent with

variations in the domain orientations between the opposing membranes given that the gel phase domains contribute ~50% of the membrane surface.

Our finding conflicts Y. Sakuma's discovery.[25] Y. Sakuma *at. el.* found the adhesion of the binary giant unilamellar vesicles composed of the negative spontaneous curvature phospholipid (NP) and zero spontaneous curvature phospholipid (ZP) happened in NP rich domains. In our case, DPPE is NP, and DOPC is ZP. The magnitude of adhesion should have been closed to pure DPPE based on Y. Sakuma's paper, which was significantly less than this expectation. We believe this was due to the structure of DPPE/DOPC mixed lipids, which is discussed above.

Single-component saturated lipids have been shown to form a relatively defect-free uncharged supported membrane on mica.[63] It was further verified by AFM scans that the average depth of all the defects (only found in 3:7 composition in AFM) was 2.0 ± 0.2 nm, comparable to the thickness of DPPE and/or DOPC molecule calculated from isotherm results. This indicated the defects were not through the whole bilayer membranes to the underlying mica substrate which was, therefore, well screened by DPPE inner monolayer.

In spite of neutral in charge of saturated lipids suggested by ionization constants in pH ~6 (the experimental condition),[64, 65] unsaturated lipids have been reported to contain small amount of charged contaminant lipids that produces a weakly charged

membrane.[60] With the origin of charge at the membrane interface, the resulting 3.8 mC/m^2 corresponds to about 1 charge per 100 lipids for 1:1 DPPE:DOPC and 2.5 mC/m^2 corresponds to about 1 charge per 160 lipids for 3:7 DPPE:DOPC. Zeta-potential measurements were carried out to make comparison with SFA results. More negatively charged vesicles were discovered in 1:1 DPPE:DOPC (-16.75 ± 4.62 mV) than 3:7 DPPE:DOPC (-10.28 ± 4.50 mV), in agreement with SFA results that 1:1 DPPE:DOPC has higher charge density than 3:7 DPPE:DOPC. Moreover, these findings suggest the charged contaminants are present in both saturated and unsaturated lipids, which were previously discovered by J. Kurniawan.[30] These also strongly suggested DPPE was more easily to get contaminated as the fact based on these two compositions that the charge density of DPPE was nearly 30 times as of DOPC.

4.2 Structures of DPPE domains and DOPC region

Based on height differences and length measurement data obtained from AFM 2D and 3D images, we created cartoon of the structure of mixed lipids in outer layer, shown in Figure 4.1. Transition region between DPPE domain and DOPC fluid region was found to be ~0.5-0.9 μm. The height difference between DPPE domain and DOPC region is ~1.5 nm.

As measured by AFM, the height difference between the solid (DPPE) and fluid (DOPC) phases was 1.5 ± 0.3 nm for the 1:1 DPPE:DOPC mixture. For both mixtures,

the experimentally measured height difference is greater than the height difference calculated from area per molecule and chemical structure (Eq. 1, ~0.7nm). This is expected as the anhydrous thickness calculation does not account for water of hydration nor the higher compressibility of the fluid phase during contact mode imaging.[66-68] Further, based on the good agreement of the area fraction, especially in the 1:1 DPPE:DOPC mixture, and use of a well packed, solid phase DPPE inner leaflet, we do not believe that there is significant flip-flop between the two leaflets. Instead we attribute the additional height difference due to a combination of the lower transfer ratio – yielding a larger area per molecule in the fluid phase, hydration of the lipid headgroups, and greater compressibility of the fluid phase. [69]

Due to the height difference between DPPE domain and DOPC region, there was a transition region in between. This mismatched transition region was found to be able to increase hydrophobic attractions [25] which was not discovered in our work. No indications showed that in supported membranes, this mismatch would destabilize the membrane and thus no fusion occurs in lipid molecules.

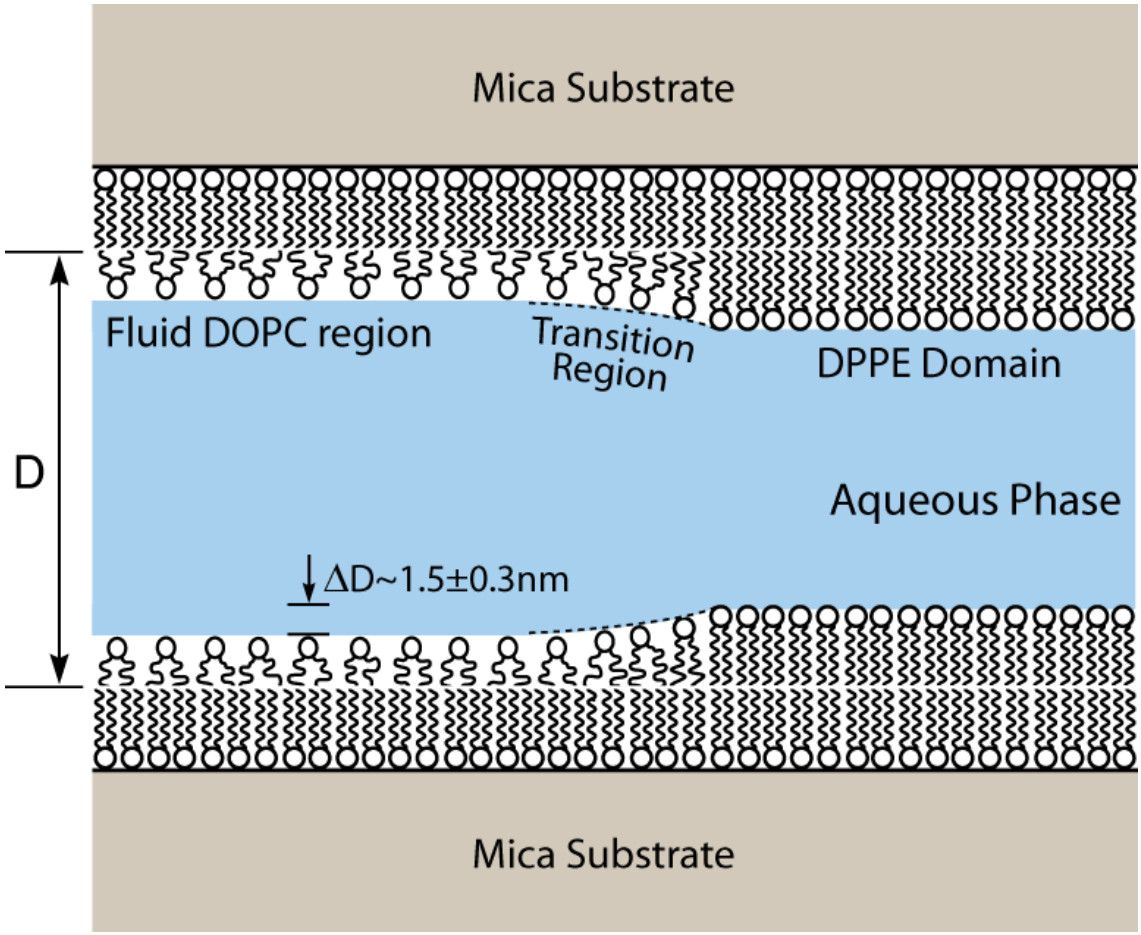

Figure 4.1 Cartoon of mixed lipids' structure. Transition region between DPPE domain and DOPC fluid region is ~0.5-0.9 μm. The height difference between DPPE domain and DOPC region is ~1.3 nm.

Transition region in 1:1 DPPE:DOPC membrane was shorter than 3:7 DPPE:DOPC membrane, as a result of larger space between DPPE domains in 3:7 mixture than 1:1 mixture. More interestingly, the dimension of transition region was much greater than our expectation. This long-range "buffer zone" can tremendously decrease the energy differences caused by the height difference. It might be the scan speed of AFM was

fast that caused the delay in response of height variation. Further slow scans will be done to deeply investigate this phenomenon.

Karttunen *et al.*[70] discovered the impact of the length of N-acylchain on lateral domain segregation and further on the morphology of the domains. Larger driving forces were found for longer acylchains for the liquid-gel phase transition at fixed surface pressure because of the van der Waals interaction between the chains. The morphology was thus governed by many small domains, which nucleated rapidly and do not grow large enough to display irregular growth morphologies. On the other hand, in the case of medium length of acylchains, the rate of growth of domains was limited by the diffusion of the component in gel-phase away from the growth front, in our case is DPPE molecules. Such diffusion-limited phase transformation processes were known to exhibit irregular growth morphologies.[71] The morphology differences between these two compositions in our case can also be explained by this mechanism. Domain morphologies obtained by AFM and FM are consistent for both compositions.[72] The flower shaped domains are consistent with diffusion-limited domain formation which is known to exhibit irregular growth morphologies.[70] Mullins and Sekerka first demonstrated that the growth front is morphologically unstable and in the case of an anisotropic capillary length, dendritic structures are observed.[71] The difference in domain morphology between the 3:7 and 1:1 mixtures is not attributed to a difference in line tension, but a kinetic effect. The higher ratio of DPPE results in effectively a more rapid compression of the monolayer and inhibits the formation of larger, flowering domains.

The height difference between DPPE domains and DOPC region obtained by AFM and isotherm gave different results. We have made some hypotheses to explain this phenomena. One possible reason is budding processes[73] in bilayer membranes which was first identified by Lipowsky, who recognized that the competition between line tension and the bending energy of the domain determined budding processes in membranes comprised of a mixture of amphiphilic molecules.[74, 75] In our case, samples for AFM were prepared as bilayers which could possibly have budding processes and make the height difference larger. However, samples for isotherm were monolayer, which could not trigger the budding processes and thus the height difference measured using different methods were different.

Another hypothesis is due to lower transfer ratio of outer layers on samples for AFM. The decrease in transfer from 1 to 0.9 would drop the estimated thickness of the fluid phase from 1.9 to 1.6nm, and thus increase the height difference between DPPE domains and DOPC region.

The dimension of transition region and its influence on membrane interactions still remain unclear and future work needs to be done to investigate deeply on this special structure. Other possible reason that this transition region exits is due to the fast scan of AFM and slow scan speed might give different dimension of this transition region. Future work could focus on all these possibilities.

Conclusion

The properties of substrate-supported lipid membrane systems have been broadly studied due to their ease of handling and compatibility with numerous surface-sensitive techniques. In this work, different ratios of mixed saturated and unsaturated lipid membranes were studied using AFM, FM and SFA. The measured membrane-membrane interaction forces were deconvolved into the respective van der Waals attraction and electrostatic repulsion. The electrostatic charge of the mixed membranes was confirmed by zeta potential measurements of similarly composed vesicles. The variation in membrane adhesion at contact was attributed to different ratios of contacting solid domains between the opposing membranes. In all cases, the measured adhesion was within the range between adhesion of pure PE-PE interaction and PC-PC interaction, based on the membrane domain surface coverage. The differences in domain morphology between the two compositions was attributed to a kinetic effect where the growth of more flower like domains due to differences in line tension was suppressed by rapid nucleation in the mixture with a greater DPPE and thereby solid phase. The presence of unexpected charges in both saturated and unsaturated lipids as a result of charged contaminant lipids, differences in domain morphology and differences in interactions with different domain ratios could be important in other supported membrane systems and should be accounted for when using mixed membrane systems in biotechnological applications.

Reference

[1] M. Tanaka, E. Sackmann, Nature, 437 (2005) 656-663.

[2] C.M. Cohen, D.I. Kalish, B.S. Jacobson, D. Branton, Journal of Cell Biology, 75 (1977) 119-134.

[3] T.M. Bayerl, M. Bloom, Biophysical Journal, 58 (1990) 357-362.

[4] R. Bruinsma, A. Behrisch, E. Sackmann, Physical Review E, 61 (2000) 4253-4267.

[5] G. Ashkenasy, D. Cahen, R. Cohen, A. Shanzer, A. Vilan, Accounts of Chemical Research, 35 (2002) 121-128.

[6] V. Borisenko, T. Lougheed, J. Hesse, E. Fureder-Kitzmuller, N. Fertig, J.C. Behrends, G.A. Woolley, G.J. Schutz, Biophysical Journal, 84 (2003) 612-622.

[7] M.M. Baksh, M. Jaros, J.T. Groves, Nature, 427 (2004) 139-141.

[8] B.A. Cornell, V.L.B. BraachMaksvytis, L.G. King, P.D.J. Osman, B. Raguse, L. Wieczorek, R.J. Pace, Nature, 387 (1997) 580-583.

[9] W.C. Lin, C.D. Blanchette, T.V. Ratto, M.L. Longo, Biophysical Journal, 90 (2006) 228-237.

[10] A. Engel, D.J. Muller, Nature Structural Biology, 7 (2000) 715-718.

[11] Y. Ebara, Y. Okahata, Journal of the American Chemical Society, 116 (1994) 11209-11212.

[12] J.M. Crane, V. Kiessling, L.K. Tamm, Langmuir : the ACS journal of surfaces and colloids, 21 (2005) 1377-1388.

[13] E.T. Castellana, P.S. Cremer, Surface Science Reports, 61 (2006) 429-444.

[14] W. Knoll, Rev. Mol. Biotechnol., 74 (2000) 137-158.

[15] E. Sackmann, M. Tanaka, Trends Biotechnol., 18 (2000) 58-64.

[16] M.L. Wagner, L.K. Tamm, Biophys. J., 61 (2001) 266-275.

[17] B.R. Lentz, Y. Barenholz, T.E. Thompson, Biochemistry, 15 (1976) 4529-4537.

[18] R. Kwok, E. Evans, Biophysical Journal, 35 (1981) 637-652.

[19] G.V. Kozlov, A.A. Volkov, J.F. Scott, G.E. Feldkamp, J. Petzelt, Physical Review B, 28 (1983) 255-261.

[20] S. Komura, D. Andelman, Europhysics Letters, 64 (2003) 844-850.

[21] J. Heuvingh, F. Pincet, S. Cribier, European Physical Journal E, 14 (2004) 269-276.

[22] W. Helfrich, Zeitschrift Fur Naturforschung Section a-a Journal of Physical Sciences, 33 (1978) 305-315.

[23] L.J. Lis, M. McAlister, N. Fuller, R.P. Rand, V.A. Parsegian, Biophysical Journal, 37 (1982) 657-665.

[24] R. Lipowsky, S. Leibler, Physical Review Letters, 56 (1986) 2541-2544.

[25] Y. Sakuma, M. Imai, M. Yanagisawa, S. Komura, The European physical journal. E, Soft matter, 25 (2008) 403-413.

[26] R.G.W. Anderson, K. Jacobson, Science, 296 (2002) 1821-1825.

[27] A.K. Kenworthy, M. Edidin, Journal of Cell Biology, 142 (1998) 69-84.

[28] L.J. Pike, Journal of Lipid Research, 44 (2003) 655-667.

[29] E.C. Lai, Journal of Cell Biology, 162 (2003) 365-370.

[30] J. Kurniawan, N.N. Yin, G.Y. Liu, T.L. Kuhl, Langmuir : the ACS journal of surfaces and colloids, 30 (2014) 4997-5004.

[31] S. Garcia-Manyes, F. Sanz, Biochimica Et Biophysica Acta-Biomembranes, 1798 (2010) 741-749.

[32] R.P. Richter, A. Brisson, Langmuir : the ACS journal of surfaces and colloids, 19 (2003) 1632-1640.

[33] S.L. Veatch, S.L. Keller, Biochimica Et Biophysica Acta-Molecular Cell Research, 1746 (2005) 172-185.

[34] B.L. Stottrup, D.S. Stevens, S.L. Keller, Biophysical Journal, 88 (2005) 269-276.

[35] R. Orozco-Alcaraz, T.L. Kuhl, Langmuir : the ACS journal of surfaces and colloids, 28 (2012) 7470-7475.

[36] N.W. Moore, T.L. Kuhl, Langmuir : the ACS journal of surfaces and colloids, 22 (2006) 8485-8491.

[37] D. Leckband, J. Israelachvili, Quarterly Reviews of Biophysics, 34 (2001) 105-267.

[38] J. Marra, J. Israelachvili, Biochemistry, 24 (1985) 4608-4618.

[39] J.N. Israelachvili, G.E. Adams, Journal of the Chemical Society-Faraday Transactions I, 74 (1978) 975-&.

[40] Israelac.Jn, Journal of Colloid and Interface Science, 44 (1973) 259-272.

[41] T.L. Kuhl, D.E. Leckband, D.D. Lasic, J.N. Israelachvili, Biophysical Journal, 66 (1994) 1479-1488.

[42] J.T.G. Overbeek, M.J. Sparnaay, Journal of Colloid Science, 7 (1952) 343-345.

[43] D. Tabor, Winterto.Rh, Proceedings of the Royal Society of London Series a-Mathematical and Physical Sciences, 312 (1969) 435-&.

[44] http://www.chemengr.ucsb.edu/

[45] D.A. Brown, E. London, Annual Review of Cell and Developmental Biology, 14 (1998) 111-136.

[46] M. Edidin, Annual Review of Biophysics and Biomolecular Structure, 32 (2003) 257-283.

[47] H.M. McConnell, M. Vrljic, Annual Review of Biophysics and Biomolecular Structure, 32 (2003) 469-492.

[48] P.F.F. Almeida, A. Pokorny, A. Hinderliter, Biochimica et Biophysica Acta (BBA) - Biomembranes, 1720 (2005) 1-13.

[49] C. Dietrich, L.A. Bagatolli, Z.N. Volovyk, N.L. Thompson, M. Levi, K. Jacobson, E. Gratton, Biophysical Journal, 80 (2001) 1417-1428.

[50] H.J. Risselada, S.J. Marrink, Proceedings of the National Academy of Sciences of the United States of America, 105 (2008) 17367-17372.

[51] S.A. Safran, T.L. Kuhl, J.N. Israelachvili, Biophysical Journal, 81 (2001) 659-666.

[52] D.R. Fattal, A. Benshaul, Biophysical Journal, 65 (1993) 1795-1809.

[53] J.F. Tocanne, L. Cezanne, A. Lopez, B. Piknova, V. Schram, J.F. Tournier, M. Welby, Chemistry and Physics of Lipids, 73 (1994) 139-158.

[54] A.J. Garcia-Saez, S. Chiantia, P. Schwille, Journal of Biological Chemistry, 282 (2007).

[55] http://www.chemicalbook.com/

[56] M.-P. Mingeot-Leclercq, M. Deleu, R. Brasseur, Y.F. Dufrene, Nature Protocols, 3 (2008) 1654-1659.

[57] http://gwyddion.net

[58] D.M. Small, Journal of Lipid Research, 8 (1967) 551-&.

[59] D.F. Kienle, J.V. de Souza, E.B. Watkins, T.L. Kuhl, Anal. Bioanal. Chem., 406 (2014) 4725-4733.

[60] F. Pincet, S. Cribier, E. Perez, European Physical Journal B, 11 (1999) 127-130.

[61] A. Hemmerle, L. Malaquin, T. Charitat, S. Lecuyer, G. Fragneto, J. Daillant, Proceedings of the National Academy of Sciences of the United States of America, 109 (2012) 19938-19942.

[62] The solid phase domain morphology was observed to change over time in monolayers at the air water interface. We ascribe these changes primarily to degredation and laibilness of unsaturated DOPC by oxygen over time.

[63] T. Kuhl, Y.Q. Guo, J.L. Alderfer, A.D. Berman, D. Leckband, J. Israelachvili, S.W. Hui, Langmuir : the ACS journal of surfaces and colloids, 12 (1996) 3003-3014.

[64] F.C. Tsui, D.M. Ojcius, W.L. Hubbell, Biophysical Journal, 49 (1986) 459-468.

[65] M.R. Moncelli, L. Becucci, R. Guidelli, Biophysical Journal, 66 (1994) 1969-1980.

[66] C.A. Helm, H. Mohwald, K. Kjaer, J. Alsnielsen, Biophysical Journal, 52 (1987) 381-390.

[67] W. Schrader, H. Ebel, P. Grabitz, E. Hanke, T. Heimburg, M. Hoeckel, M. Kahle, F. Wente, U. Kaatze, Journal of Physical Chemistry B, 106 (2002) 6581-6586.

[68] C. Das, K.H. Sheikh, P.D. Olmsted, S.D. Connell, Physical Review E, 82 (2010).

[69] The decrease in transfer ratio from 1 to 0.9 would drop the estimated thickness of the fluid phase from 1.9 to 1.6nm, and thus increase the height difference.

[70] M. Karttunen, M.P. Haataja, M. Saily, I. Vattulainen, J.M. Holopainen, Langmuir : the ACS journal of surfaces and colloids, 25 (2009) 4595-4600.

[71] W.W. Mullins, R.F. Sekerka, Journal of Applied Physics, 34 (1963) 323-&.

[72] Domains show more round-shaped in FM than AFM for 1:1 composition due to lower resolution and the larger scale. Zoomed-in figures show similar domain morphologies (jagged shape).

[73] I. Sriram, D.K. Schwartz, Surface Science Reports, 67 (2012) 143-159.

[74] R. Lipowsky, Journal De Physique Ii, 2 (1992) 1825-1840.

[75] R. Lipowsky, Biophysical Journal, 64 (1993) 1133-1138.